THE ASTROPHYSICAL JOURNAL, 526:215–235, 1999 November 20
© 1999. The American Astronomical Society. All rights reserved. Printed in U.S.A.

COSMIC ANTIPROTONS AS A PROBE FOR SUPERSYMMETRIC DARK MATTER?

LARS BERGSTRÖM, JOAKIM EDSJÖ, AND PIERO ULLIO
Department of Physics, Stockholm University, Box 6730, SE-113 85 Stockholm, Sweden; lbe@physto.se, edsjo@physto.se, piero@physto.se
Received 1999 February 1; accepted 1999 July 8

ABSTRACT

The flux of cosmic-ray antiprotons from neutralino annihilations in the Galactic halo is computed for a large sample of models in the minimal supersymmetric extension of the standard model (MSSM). We also revisit the problem of estimating the background of low-energy cosmic-ray–induced secondary antiprotons, taking into account their subsequent interactions (and energy loss) and the presence of nuclei in the interstellar matter. We consider a two-zone diffusion model, with and without a Galactic wind. We find that, given the uncertainties in the background predictions, there is no need for a primary (exotic) component to explain current data. However, allowing for a signal by playing with the uncertainties in the background estimate, we discuss the characteristic features of the supersymmetric models that give a satisfactory description of the data. We point out that in some cases, the optimal kinetic energy to search for a signal from supersymmetric dark matter is above several GeV, rather than the traditional sub-GeV region. The large astrophysical uncertainties involved do not, on the other hand, allow the exclusion of any of the MSSM models we consider on the basis of data. In addition to numerical results, we also present convenient parameterizations of the antiproton yields of all "basic" two-body final states. We also give examples of the yield and differential energy spectrum for a set of supersymmetric models with high rates. We also remark that it is difficult to set a limit on the antiproton lifetime from present measurements, since the injection of antiprotons from neutralino annihilation can compensate for the loss from decay.

Subject headings: cosmic rays — dark matter — diffusion — elementary particles — Galaxy: halo

1. INTRODUCTION

The mystery of the dark matter in the universe remains unsolved. Among the most plausible candidates are weakly interacting massive particles (WIMPs), of which the supersymmetric neutralino is a favorite candidate from the point of view of particle physics. The neutralino arises naturally in supersymmetric extensions of the standard model, and has the attractive feature of giving a relic density which in large regions of parameter space is adequate to explain cosmological dark matter. We will in this paper consider the neutralino as a dark matter candidate within the minimal supersymmetric extension of the standard model (MSSM). For a thorough review of neutralino dark matter, see Jungman, Kamionkowski, & Griest (1996).

Neutralino dark matter can be and is searched for in several ways: directly through detection of nuclear recoils and/or ionization in direct detection experiments, and indirectly through searches for their annihilation products from annihilations in the Earth or Sun (for neutrinos) and the Galactic halo. In this paper, we discuss the detection prospects for antiprotons from neutralino annihilation in the Galactic halo.

Since antimatter seems not to exist in large quantities in the observable universe, including our own Galaxy, any contribution to the cosmic-ray–generated antimatter flux (apart from antiprotons and positrons) from exotic sources may in principle be a good signature for such sources. Since neutralinos are constrained by supersymmetry to be Majorana fermions, they are their own antiparticles, and therefore the final state in their annihilations in the halo will contain equal amounts of matter and antimatter (given the particle physics constraints on CP-violating couplings and in particular on baryon number violation). The excess of particles would drown in the background of particles from astrophysical sources, but there is a chance that antiparticles from this new primary source could be detectable. This issue has recently come into new focus thanks to upcoming space experiments such as PAMELA (Adriani et al. 1995) and AMS (Ahlen et al. 1994), with increased sensitivity to the cosmic antimatter flux.

Cosmic-ray–induced secondary antiprotons are generated mainly through $pp \rightarrow \bar{p} + X$ collisions of cosmic-ray protons with interstellar matter. For kinematical reasons they are born with a nonzero momentum. The strategy to search for exotic signals has thus been to investigate the low-energy region, since, e.g., a neutralino-induced component does not drop as fast at low energies. However, as we will see, this ideal picture is blurred to a large extent by a "tertiary" component caused by scattering with energy loss of the secondary antiprotons. In addition, heavier nuclei in the interstellar medium target (primarily helium) cause a significant antiproton flux at low energy. In particular, it is known that in proton-nucleus collisions, antiprotons may be produced well below the nominal pp energy threshold. In addition, low-energy particles have difficulties entering the heliosphere, which makes the connection of the measured fluxes to the interstellar ones dependent on a not completely known correction due to this solar modulation (which follows the 11 yr solar cycle).

Using reasonable parameters for the computation of all these effects, we will show that we are able to explain in a satisfactory way the present experimental data on cosmic-ray antiprotons without the need of a primary component. This is seen in Figure 1, where our computed reference distribution for the background is compared to the recent data from the BESS experiment (BESS 95, Matsunaga et al. 1998; BESS 97, Orito 1999). The satisfactory agreement can be compared to the conclusions of a recent analysis (Bottino et al. 1998) in which the need for an exotic component was more apparent. The main cause of this difference lies in our improved treatment of energy loss during propagation and our inclusion of the helium

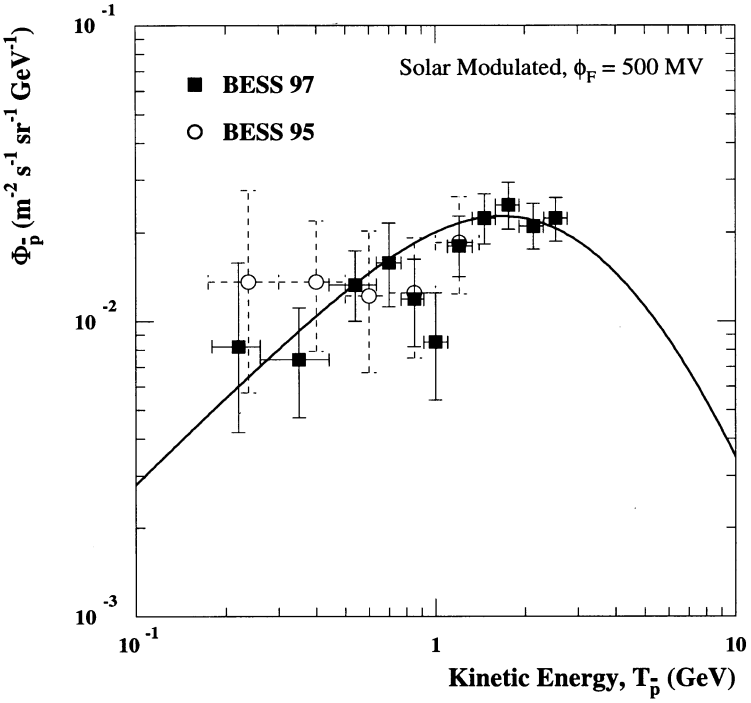

FIG. 1.—Background of antiprotons, solar modulated with $\phi_F = 500$ MV. The BESS 95 and 97 data are also shown (Matsunaga et al. 1998; Orito 1999).

component of the interstellar medium. From Figure 1 one can also see that the more recent BESS data (Orito 1999) indicate a lower flux at low energy than earlier data. If reacceleration effects were included, the need for an exotic component would be even less.

It is, however, also evident from Figure 1 that the statistical sample of antiprotons presently available is very limited, so that a new primary component cannot yet be ruled out with high significance even if the propagation parameters were known. By varying all parameters in this complex astrophysical problem, the room for an exotic contribution can, as we will see, be made quite large, so it is certainly worthwhile to investigate what a favored dark matter candidate such as the MSSM neutralino may yield in terms of a signal. It is apparent from Figure 1 that the low-energy tail of cosmic-ray–induced antiprotons does not fall very rapidly with decreasing kinetic energy, so this particular region of phase-space may not yield as nice a signature for a dark matter neutralino as previously thought. Therefore, we will also discuss the cases (mainly for high-mass neutralinos) for which the optimal kinetic energy for finding an exotic contribution is above several GeV. Unfortunately, it will turn out that the rates in that energy region are not large enough to cause a spectral distortion, unless the background of secondary antiprotons is considerably smaller and/or the signal is considerably larger than our canonical results show. This lack of spectral features in the neutralino-induced antiproton flux causes severe fundamental limitations for this indirect method of detecting supersymmetric dark matter.

The idea of a dark matter–induced component in the cosmic antiproton spectrum has a long history. An early report (Buffington et al. 1981) of an anomalous excess of cosmic-ray antiprotons at low energies led to the suggestion that annihilation of relic neutralinos could be the source. Calculations of fluxes have since then been performed with different degrees of sophistication, ranging from order-of-magnitude estimates (Silk & Srednicki 1984) and analytical expressions (Stecker, Rudaz, & Walsh 1985) to results from Monte Carlo simulations (Ellis et al. 1988; Stecker & Tylka 1989; Jungman & Kamionkowski 1994; Bottino et al. 1995, 1997). The latter method has also been used together with $\bar{p}$ production from neutralino annihilation in a minimal supergravity scheme (Diehl et al. 1995).

In this work, we use the Lund Monte Carlo PYTHIA 6.115 (Sjöstrand 1994) to simulate the energy spectrum of antiprotons from neutralino annihilation. We have used large numerical tables for our computations, but for convenience we also present useful parameterizations of the $\bar{p}$ fluxes from various annihilation channels. In the following sections we will describe the MSSM model we use and the Monte Carlo simulations, and discuss the antiproton propagation model, the background fluxes, and the uncertainties in both the background and the signal. Finally, we will show and discuss our results.

2. DEFINITION OF THE SUPERSYMMETRIC MODEL

We work in the minimal supersymmetric standard model (MSSM). In general, the MSSM has many free parameters, but with some reasonable assumptions we can reduce the number of parameters to the Higgsino mass parameter, μ, the gaugino mass parameter, M_2, the ratio of the Higgs vacuum expectation values, tan β, the mass of the CP-odd Higgs boson, m_A (or $m_{H_3^0}$), the scalar mass parameter, m_0, and the trilinear soft SUSY-breaking parameters, A_b and A_t, for the third generation. In particular, we do not impose any restrictions from supergravity other than gaugino mass unification, which relates the other gaugino mass parameter, M_1, to M_2. (We remind the reader that one of the most attractive features of the MSSM is that, unlike the nonsupersymmetric standard model, it is compatible with gauge coupling unification given the current data on the

TABLE 1

PARAMETER VALUES USED IN OUR SCANS OF THE MSSM PARAMETER SPACE

Parameter	Minimum	Maximum
μ (GeV)	−50,000	50,000
M_2 (GeV)	−50,000	50,000
tan β	1.0	60.0
m_A	0	10,000
m_0	100	30,000
A_b/m_0	−3	3
A_t/m_0	−3	3

NOTE.—Note that several special scans aimed at interesting regions of the parameter space have been performed. In total we have generated approximately 116,000 models that obey all accelerator constraints. Of these, about 41,000 have a relic density in the range $0.025 < \Omega_\chi h^2 < 1$.

running of low-energy gauge couplings.) For a more detailed definition of the parameters and a full set of Feynman rules, we refer the reader to Edsjö & Gondolo (1997) and Edsjö (1997).

The lightest stable supersymmetric particle is in most models the lightest neutralino (which we will henceforth call simply "the neutralino," χ), which is a superposition of the superpartners of the gauge and Higgs fields,

$$\chi \equiv \tilde{\chi}_1^0 = N_{11}\tilde{B} + N_{12}\tilde{W}^3 + N_{13}\tilde{H}_1^0 + N_{14}\tilde{H}_2^0 . \tag{1}$$

It is convenient to define the gaugino fraction of the neutralino,

$$Z_g = |N_{11}|^2 + |N_{12}|^2 . \tag{2}$$

For the masses of the neutralinos and charginos, we use the one-loop corrections from the literature (Drees et al. 1997; Pierce & Papadopoulos 1994a, 1994b; Lahanas, Tamvakis, & Tracas 1994), and for the Higgs boson masses we use the leading logarithmic two-loop radiative corrections, calculated within the effective potential approach given by Carena et al. (1995).

We make extensive scans of the model parameter space, some general and some specialized to interesting regions. In total we make 22 different scans of the parameter space. The scans are done randomly and are mostly distributed logarithmically in the mass parameters and in tan β. For some scans, the logarithmic scan in μ and M_2 has been replaced by a logarithmic scan in the more physical parameters m_χ and $Z_g/(1 - Z_g)$, where m_χ is the neutralino mass. Combining all the scans, the overall limits of the seven MSSM parameters we use are given in Table 1.

We check each model to see if it is excluded by the most recent accelerator constraints, of which the most important are the LEP bounds (Carr 1998)[1] on the lightest chargino mass,

$$m_{\chi_1^+} > \begin{cases} 91 \text{ GeV}, & |m_{\chi_1^+} - m_{\chi_1^0}| > 4 \text{ GeV} \\ 85 \text{ GeV}, & \text{otherwise,} \end{cases} \tag{3}$$

and on the lightest Higgs boson mass, $m_{H_2^0}$ [which range from 72.2–88.0 GeV depending on sin $(\beta - \alpha)$, where α is a mixing angle in the Higgs sector], and the constraints from $b \to s\gamma$ (Ammar et al. 1993; Alam et al. 1995). The new higher precision measurement from CLEO (Glenn et al. 1999) gives a slightly smaller range for that process than the one we have allowed; we have checked, however, that this causes no major changes in the properties related to the $\bar{p}$ yield for the allowed models.

For each allowed model we compute the relic density of neutralinos, $\Omega_\chi h^2$, where Ω_χ is the density in units of the critical density and h is the present Hubble constant in units of 100 km s^{-1} Mpc^{-1}. We use the formalism of Gondolo & Gelmini (1991) for resonant annihilations, threshold effects, and finite widths of unstable particles, and we include all two-body tree-level annihilation channels of neutralinos. We also include the so-called coannihilation processes according to the results of Edsjö & Gondolo (1997) in the relic density calculation.

Present observations favor $h = 0.6 \pm 0.1$ and a total matter density $\Omega_M = 0.3 \pm 0.1$, of which baryons may contribute 0.02 to 0.08 (see, e.g., Schramm & Turner 1998). Not to be overly restrictive, we accept $\Omega_\chi h^2$ in the range from 0.025 to 1 as cosmologically interesting. The lower bound is somewhat arbitrary, since there may be several different components of nonbaryonic dark matter, but we demand that neutralinos are at least as abundant as required to make up the dark halos of galaxies. In principle, neutralinos with $\Omega_\chi h^2 < 0.025$ would still be relic particles, but only making up a small fraction of the dark matter of the universe. We will consider models with $\Omega_\chi h^2 < 0.025$ only when discussing the dependence of the signal on $\Omega_\chi h^2$.

It may also be of interest to consider specifically models that naturally give a value of $\Omega_\chi h^2$ close to the present "best-fit" value. We will therefore present some figures in which the range between 0.1 and 0.2 for $\Omega_\chi h^2$ is shown by special symbols.

[1] Talk by Carr (1998) is available at: http://alephwww.cern.ch/ALPUB/seminar/carrlepc98/index.html.

Since in general a small relic density implies a large annihilation cross section and vice versa, this tends to cut out a large fraction of the models with otherwise observable rates—a fact not always highlighted in previous analyses.

3. ANTIPROTON PRODUCTION BY NEUTRALINO ANNIHILATION

3.1. *Introduction*

Neutralinos are Majorana fermions and will annihilate with each other in the halo, producing leptons, quarks, gluons, gauge bosons, and Higgs bosons. The quarks, gauge bosons, and Higgs bosons will decay and/or form jets that will give rise to antiprotons (and antineutrons, which decay shortly to antiprotons).

At tree level, the relevant final states for $\bar{p}$ production will be $q\bar{q}$, $\ell\bar{\ell}$, W^+W^-, Z^0Z^0, W^+H^-, ZH_1^0, ZH_2^0, $H_1^0H_3^0$, and $H_2^0H_3^0$. We will include all the heavier quarks (c, b, and t), gauge bosons, and Higgs boson final states in our analysis. In addition, we will include the $Z\gamma$ (Ullio & Bergström 1998) and the 2 gluon (Drees et al. 1994; Bergström & Ullio 1997) final states which occur at one loop level. Note that for the antiproton-rich 2 gluon final state, the improved and corrected formulas given in the second reference generally imply a lower branching ratio than those of the former reference, which has been used in several previous analyses.

The hadronization for all final states (including gluons) is simulated with the well-known particle physics Lund Monte Carlo program PYTHIA 6.115 (Sjöstrand 1994), which is used extensively at accelerators in simulations of jet production at the full energy range that we need to consider here. A word of caution should be raised, however, that antiproton data is not very abundant, in particular not at the lowest antiproton lab energies, which tend to dominate our signal. Therefore, an uncertainty in normalization, probably of the order of a factor of 2, cannot be excluded at least in the low-energy region.

3.2. *Simulations*

To get the energy distribution of antiprotons for each of the final states listed in the previous subsection, we generate the final states $c\bar{c}$, $b\bar{b}$, $t\bar{t}$, W^+W^-, Z^0Z^0, and gg and let them decay/hadronize according to PYTHIA 6.115. We do not need to include lighter quarks, since the branching ratios to these are negligible. The annihilation channels containing Higgs bosons need not be simulated separately, since they decay to other particles that we do simulate. They are then allowed to decay in flight, and the spectra from the decay products are boosted and averaged over the decay angles. During the simulations, antineutrons are allowed to decay, since we would otherwise underestimate the flux by a factor of 2.

We have performed simulations for the neutralino masses m_χ = 10, 25, 50, 80.3, 91.2, 100, 150, 176, 200, 250, 350, 500, 750, 1000, 1500, 2000, 3000, and 5000 GeV; for intermediate masses an interpolation is used. For each mass and annihilation channel, 2.5×10^5 events have been simulated.

For easier use, we have also parameterized the antiproton distributions for the "basic" annihilation channels given above. It is for this purpose more convenient to define $x = T_{\bar{p}}/m_\chi$, with $T_{\bar{p}}$ being the kinetic energy of the antiproton, as the independent variable. A suitable parameterization is then given by

$$\frac{dN}{dx} = (p_1 x^{p_3} + p_2 |\log_{10} x|^{p_4})^{-1} , \tag{4}$$

where the parameters p_i depend on both the annihilation channel and the neutralino mass. The latter dependence is parameterized as

$$p_i(m_\chi) = (a_{i1} m_\chi^{a_{i2}} + a_{i3} m_\chi^{a_{i4}})^{-1} . \tag{5}$$

The values of the a_{ij} for the different annihilation channels are given in Table 2. These parameterizations are valid for neutralino masses in the range 50–5000 GeV. The error in the most relevant regions, i.e., the low-energy tail to most of the high-energy slope, is usually less than 20%. At worst (for $t\bar{t}$), it can be up to 50% in isolated regions. This should be compared with the uncertainties in PYTHIA, which probably can be up to a factor of 2. In Figure 2 we give as an example the distributions for a 100 GeV neutralino annihilating into $b\bar{b}$ and a 1000 GeV neutralino annihilating into W^+W^-.

Note that the above parameterizations are only given for the reader's convenience; in our calculations we use the results of the simulations directly. For convenience, we also show in Table 3 the individual branching ratios of the main modes for a set of models with high antiproton yield but different mass and gaugino content.

TABLE 2

PARAMETERS FITTED TO THE ANTIPROTON DISTRIBUTIONS FOR NEUTRALINO MASSES 50–5000 GeV

	p_1				p_2		p_3		p_4			
Channel	a_{11}	a_{12}	a_{13}	a_{14}	a_{21}	a_{22}	a_{31}	a_{32}	a_{41}	a_{42}	a_{43}	a_{44}
$c\bar{c}$	1.70	1.40	0	0	3.12	0.04	−2.22	0	−0.39	−0.076	0	0
$b\bar{b}$	1.75	1.40	0	0	1.54	0.11	−2.22	0	−0.31	−0.052	0	0
$t\bar{t}$	1.35	1.45	0	0	1.18	0.15	−2.22	0	−0.21	0	0	0
W^+W^-	306.0	0.28	7.2×10^{-4}	2.25	2.32	0.05	−8.5	−0.31	−0.39	−0.17	-2.0×10^{-2}	0.23
Z^0Z^0	480.0	0.26	9.6×10^{-4}	2.27	2.17	0.05	−8.5	−0.31	−0.33	−0.075	-1.5×10^{-4}	0.71
gg	2.33	1.49	0	0	3.85	0.06	−2.17	0	−0.312	−0.053	0	0

NOTE.The parameters a_{23}, a_{24}, a_{33}, and a_{34} are always zero and are not given in the table. The parameterized distributions are given by eqs. (4)–(5).

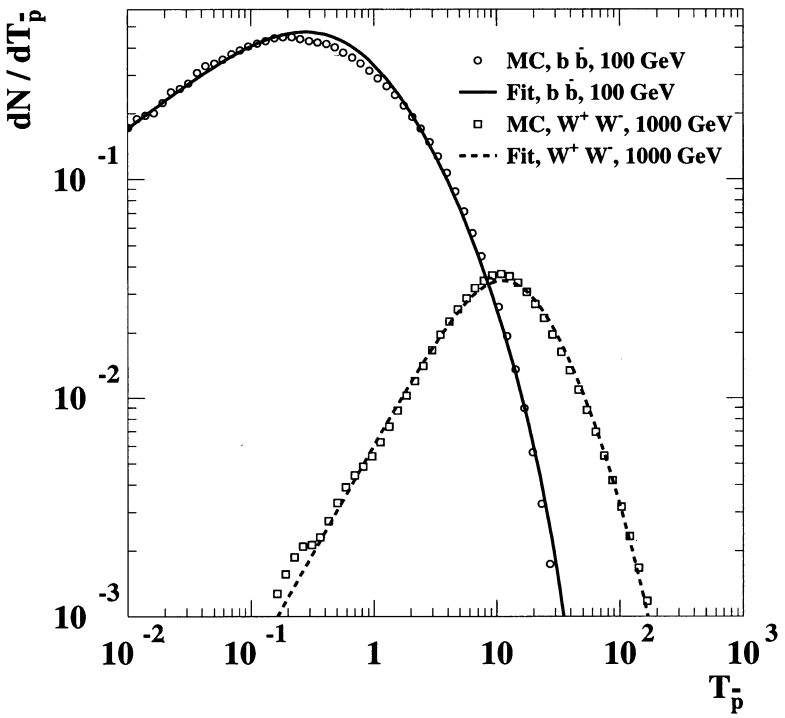

FIG. 2.—Examples of the fits to the antiproton distributions from neutralino annihilation, $dN/dT = (1/m_\chi)dN/dx$, where dN/dx is given by eqs. (4)–(5) and Table 2.

3.3. *The Antiproton Source Function*

The source function $Q_{\bar{p}}^{\chi}$ gives the number of antiprotons per unit time, energy, and volume element produced in annihilation of neutralinos locally in space. It is given by

$$Q_{\bar{p}}^{\chi}(T, x) = (\sigma_{\rm ann} v)\left[\frac{\rho_\chi(x)}{m_\chi}\right]^2 \sum_f \frac{dN^f}{dT} B^f , \tag{6}$$

where T is the $\bar{p}$ kinetic energy. For a given annihilation channel f, B^f and dN^f/dT are, respectively, the branching ratio and the fragmentation function, and $(\sigma_{\rm ann} v)$ is the annihilation rate at $v = 0$ (which is very good approximation, since the velocity of the neutralinos in the halo is so low). Since dark matter neutralinos annihilate in pairs, the source function is proportional to the square of the neutralino number density, $n_\chi = \rho_\chi/m_\chi$. Assuming that most of the dark matter in the Galaxy is made up of neutralinos and that these are smoothly distributed in the halo, one can directly relate the neutralino number density to the dark matter density profile in the Galactic halo, ρ. Given a generic parameterization of ρ, we fix

$$\rho_{\tilde{\chi}}(x) \equiv \rho(x) = \rho_0\left(\frac{r_0}{|x|}\right)^\gamma \left[\frac{1 + (r_0/a)^\alpha}{1 + (|x|/a)^\alpha}\right]^{(\beta-\gamma)/\alpha} , \tag{7}$$

where ρ_0 is the value of the local halo density, r_0 is the Galactocentric distance of the Sun, and a is some length scale; we assume $\rho_0 = 0.3$ GeV cm^{-3} and $r_0 = 8.5$ kpc. In the actual computation, we will mainly restrict ourselves to the case in which the dark matter density profile is described by a modified isothermal distribution, $(\alpha, \beta, \gamma) = (2, 2, 0)$, mentioning what changes are expected if more cuspy profiles, which are favored by results in N-body simulations of hierarchical clustering, are considered. We will in particular consider the example of the Navarro, Frenk, & White (1996) profile, $(\alpha, \beta, \gamma) = (1,2,1)$. Although we are here focusing on the case of a smooth distribution of dark matter particles in the halo, an extension to a clumpy distribution is potentially interesting as well (Bergström et al. 1999; Ullio 1999).

Given the $\bar{p}$ distributions calculated in the previous section, we can now get the source function for any given annihilation channel.

4. PROPAGATION MODEL

In the absence of a well-established theory to describe the interactions of charged particles with the magnetic field of the Galaxy and the interstellar medium, the propagation of cosmic rays has generally been treated by postulating a semiempirical model and fitting the necessary set of unknown parameters to available data. A common approach is to use a diffusion approximation defined by a transport equation and an appropriate choice of boundary conditions (see, e.g., Berezinskii et al. 1990; Gaisser 1990 and references therein).

In most diffusion models, the form of the terms present in the diffusion equation is a compromise between physical insight and the possibility of an analytical solution. Only recently have more realistic models been studied by applying numerical solutions (Strong & Moskalenko 1998) or Monte Carlo simulations (Porter & Protheroe 1997).

TABLE 3

EXAMPLES OF MODELS GIVING HIGH ANTIPROTON RATES

Parameter	1	2	3	4	5	6	7
μ	926.6	−191.2	708.7	−127.6	−543.1	−891.2	379.6
M_2	92.4	−149.8	−2156.1	242.3	413.3	111.5	−162.4
tan β	19.1	45.1	9.67	5.09	4.17	38.6	28.8
m_A	79.8	543.3	1405.0	1838.5	409.2	77.9	89.5
m_0	922.5	306.6	2817.0	4243.2	1054.6	1110.6	1109.1
A_b/m_0	0.95	0.17	−2.05	1.22	−1.28	0.17	1.84
A_t/m_0	−2.11	0.96	0.46	−0.38	−1.72	2.06	−2.20
m_{χ^0}	46.2	69.4	704.9	98.9	208.2	56.1	80.9
Z_g	0.99761	0.88843	0.00642	0.37943	0.99293	0.99756	0.98440
m_{χ^+}	91.0	117.9	708.3	123.8	405.8	110.9	155.7
$m_{H_1^0}$	126.6	543.3	1405.2	1838.9	412.0	126.8	127.4
$m_{H_2^0}$	76.7	107.5	117.8	115.5	115.5	76.2	89.0
$m_{H^\pm}$	111.5	549.7	1407.1	1840.1	416.4	115.5	120.0
$(\sigma_{\rm ann} v)$	0.127	0.0874	0.420	0.0719	0.116	0.0824	0.0785
Br($c\bar{c}$)	$<10^{-5}$	0.00001	$<10^{-5}$	0.00050	0.00007	$<10^{-5}$	$<10^{-5}$
Br($b\bar{b}$)	0.96	0.98	0.81	0.0059	0.32	0.96	0.96
Br($t\bar{t}$)	...	...	0.11	...	0.65	...	...
Br(W^+W^-)	...	...	0.024	0.87	$<10^{-5}$	...	$<10^{-5}$
Br(Z^0Z^0)	...	...	0.020	0.12	$<10^{-5}$	...	...
Br(gg)	0.00060	0.0028	0.00017	0.0016	0.0028	0.00054	0.00043
Br($\gamma\gamma$)	3.7×10^{-7}	3.9×10^{-6}	6.5×10^{-5}	1.8×10^{-4}	2.3×10^{-6}	9.6×10^{-7}	1.2×10^{-6}
Br($Z\gamma$)	5.8×10^{-13}	5.8×10^{-6}	1.7×10^{-4}	6.5×10^{-4}	2.3×10^{-5}	6.3×10^{-10}	2.1×10^{-6}
$\Omega_\chi h^2$	0.025	0.028	0.032	0.025	0.050	0.034	0.034
$\Phi_{\bar{p}}$	4.6×10^{-2}	1.6×10^{-2}	8.5×10^{-4}	8.8×10^{-3}	4.0×10^{-3}	2.1×10^{-2}	1.1×10^{-2}
$\Phi_{\mu,\rm Earth}$	3.8×10^{-1}	1.0×10^{0}	2.4×10^{-5}	1.1×10^{-2}	2.5×10^{-7}	7.5×10^{1}	2.3×10^{1}
$\Phi_{\mu,\rm Sun}$	7.0×10^{-2}	2.6×10^{0}	4.1×10^{-1}	2.7×10^{3}	8.7×10^{-1}	1.3×10^{0}	1.8×10^{1}
$\sigma_{\rm SI}$	2.9×10^{-7}	4.0×10^{-7}	9.6×10^{-10}	1.2×10^{-8}	1.2×10^{-10}	1.2×10^{-6}	2.3×10^{-6}
Φ_{e^+}	5.0×10^{-8}	2.9×10^{-8}	3.2×10^{-8}	2.6×10^{-8}	2.0×10^{-8}	3.1×10^{-8}	2.6×10^{-8}
$\Phi_{\rm cont.,\gamma}$	8.1×10^{-8}	3.5×10^{-8}	5.9×10^{-9}	1.4×10^{-8}	1.1×10^{-8}	4.2×10^{-8}	2.6×10^{-8}

NOTE.—All masses are given in GeV; the annihilation rate is given in 10^{-24} cm^3 s^{-1}; the solar modulated $\bar{p}$ flux at 0.35 GeV is in m^{-2} s^{-1} sr^{-1} sr^{-1}; the neutrino flux from the Earth and the Sun is with a threshold of 25 GeV and in units of km^{-2} yr^{-1}; the spin-independent cross section is in pb; the solar modulated positron flux is in one of the HEAT bins (8.9–14.8 GeV) and in units of cm^{-2} s^{-1} sr^{-1} GeV^{-1}; the continuum gamma flux is for high Galactic latitudes and is given in cm^{-2} s^{-1} sr^{-1}, integrated above 1 GeV. The rates and fluxes are calculated as given in Bergström & Gondolo 1996, Bergström et al. 1999, Baltz & Edsjö 1999, and Bergström et al. 1998b, 1998a.

Our analysis is focused on comparing the characteristics of cosmic-ray antiproton signals of different origin: secondary antiprotons produced in cosmic-ray interactions and, eventually, a primary flux from neutralino annihilations. In particular, we want to examine the dependence of the relative strength and spectral signatures on the diffusion model and the distribution of particle dark matter in the Galactic halo. Since both of these are not well constrained, we believe that an analytic solution of a reasonable physical model will be sufficient to provide most of the information needed on the behavior of the two types of signals.

We choose to describe the propagation of cosmic rays in the Galaxy by a transport equation of the diffusion type as written by Ginzburg & Syrovatskii (1964; see also Berezinskii et al. 1990; Gaisser 1990). In the case of a stationary solution, the number density N of a stable cosmic-ray species whose distribution of sources is defined by the function of energy and space $Q(E, \boldsymbol{x})$ is given by

$$\frac{\partial N(E, \boldsymbol{x})}{\partial t} = 0 = \nabla \cdot [D(R, \boldsymbol{x}) \nabla N(E, \boldsymbol{x})] - \nabla \cdot [\boldsymbol{u}(\boldsymbol{x}) N(E, \boldsymbol{x})] - p(E, \boldsymbol{x}) N(E, \boldsymbol{x}) + Q(E, \boldsymbol{x}) \, . \tag{8}$$

Here and below we try to keep the notation as general as possible. Although our goal is to compute N for antiprotons, in order to determine the source function for the secondary flux, we will have to obtain the spatial density distribution for protons as well. On the right-hand side of equation (8), the first term implements the diffusion approximation for a given diffusion coefficient D, generally assumed to be a function of rigidity, R, while the second term describes a large-scale convective motion of velocity $\boldsymbol{u}$. The third term is added to take into account losses of cosmic rays due to collisions with the interstellar matter. It is a very good approximation to include in this term only the interactions with interstellar hydrogen (on the other hand, we will point out below that heavier elements, in particular helium, cannot be neglected when computing the source function for secondary antiprotons); in this case, p is given by

$$p(E, \boldsymbol{x}) = n^{\rm H}(\boldsymbol{x}) v(E) \sigma^{\rm in}_{{\rm cr}\ p}(E) \tag{9}$$

where $n^{\rm H}$ is the hydrogen number density in the Galaxy, v is the velocity of the cosmic-ray particle considered, "cr," and $\sigma^{\rm in}_{{\rm cr}p}$ is the inelastic cross section for cr-proton collisions. In equation (8) we have neglected continuous energy losses; this will be included in an implicit form when considering secondary antiprotons. We briefly mention in the conclusions the possibility

that antiprotons have a finite lifetime, τ. To take this effect into account, the term $-(1/\tau)N(E, \boldsymbol{x})$ should be added on the right-hand side of equation (8), which corresponds to shifting p to $p + 1/\tau$ in all the equations below.

We now must specify the parameters introduced and the boundary conditions. We mainly follow the approach of Ginzburg, Khazan, & Ptuskin (1980), given also in Berezinskii et al. (1990), and analogous to that of Webber, Lee, & Gupta (1992), Chardonnet et al. (1996), and Bottino et al. (1998). The main feature is that the propagation region is assumed to have a cylindrical symmetry: the Galaxy is split into two parts, a disk of radius R_h and height $2h_g$, where most of the interstellar gas is confined, and a halo of height $2h_h$ and the same radius. We assume that the diffusion coefficient is isotropic, with possibly two different values in the disk and in the halo, reflecting the fact that in the disk there may be a larger random component of the magnetic fields. We then have a spatial dependence

$$D(\boldsymbol{x}) = D(z) = D_g\,\theta(h_g - |z|) + D_h\,\theta(|z| - h_g)\ . \tag{10}$$

Regarding the rigidity dependence, fits to cosmic-ray data in models that do not include reacceleration effects indicate that D scales as $R^{0.6}$ (Webber et al. 1992; Strong & Moskalenko 1998), with a cutoff below some rigidity R_0. We consider the same functional form as in Chardonnet et al. (1996) and Bottino et al. (1998),

$$D_l(R) = D_l^0\left(1 + \frac{R}{R_0}\right)^{0.6}\ , \tag{11}$$

where $l = g, h$. We will briefly discuss below what changes are expected if reacceleration is included, without making numerical predictions. The convective term has been introduced in equation (8) to describe the effect of particle motion against the wind of cosmic rays leaving the disk. We will therefore not consider any convection in the radial direction, assuming instead a Galactic wind of velocity

$$\boldsymbol{u}(\boldsymbol{x}) = (0,\ 0,\ u(z)) \tag{12}$$

where

$$u(z) = \mathrm{sign}(z)u_h\,\theta(|z| - h_g)\ . \tag{13}$$

An analytic solution is also possible in the case of a linearly increasing wind (Ullio 1999). The last parameter we need to specify is the distribution of gas in the Galaxy; for convenience, we assume that this has the very simple z dependence

$$n^{\mathrm{H}}(\boldsymbol{x}) = n^{\mathrm{H}}(z) = n_g^{\mathrm{H}}\,\theta(h_g - |z|) + n_h^{\mathrm{H}}\,\theta(|z| - h_g)\ , \tag{14}$$

where $n_h \ll n_g$ (in practice we will take $n_h = 0$), and an average in the radial direction is performed. Finally, since we eventually want to treat the case of clumpy neutralino dark matter (Ullio 1999), we will not assume any symmetry in the source function $Q(\boldsymbol{x})$ (note that to apply the results of this section to sources with a cylindrical symmetry, as for instance eq. [6] with the assumption in eq. [7], it is sufficient to set everywhere the index k equal to 0).

As a boundary condition, it is usually assumed that cosmic rays can escape freely at the border of the propagation region, i.e.,

$$N(R_h, z) = N(r, h_h) = N(r, -h_h) = 0\ , \tag{15}$$

since the density of cosmic rays is assumed to be negligibly small in the intergalactic space. To check whether this hypothesis holds even in the case of a source from dark matter annihilations, we will compare the flux of outgoing antiprotons with that entering the diffusion region due to sources in "free space." For references regarding other possible choices of boundary conditions, see Berezinskii et al. (1990).

The cylindrical symmetry and the free escape at the boundaries make it possible to solve the transport equation by expanding the number density distribution N in a Fourier-Bessel series,

$$N(r, z, \theta) = \sum_{k=0}^{\infty}\sum_{s=1}^{\infty} J_k\left(v_s^k\,\frac{r}{R_h}\right)[M_s^k(z)\cos(k\theta) + \tilde{M}_s^k(z)\sin(k\theta)]\ , \tag{16}$$

which automatically satisfies the boundary condition at $r = R_h$, where v_s^k is the sth zero of J_k (the Bessel function of the first kind and of order k). In the same way, the source function can be expanded as

$$Q(r, z, \theta) = \sum_{k=0}^{\infty}\sum_{s=1}^{\infty} J_k\left(v_s^k\,\frac{r}{R_h}\right)[Q_s^k(z)\cos(k\theta) + \tilde{Q}_s^k(z)\sin(k\theta)]\ , \tag{17}$$

where

$$Q_s^k(z) = \frac{2}{R_h^2\,J_{k+1}^2(v_s^k)}\int_0^{R_h} dr'\,r'J_k\left(v_s^k\,\frac{r'}{R_h}\right)\frac{1}{\alpha_k\,\pi}\int_{-\pi}^{\pi} d\theta'\cos(k\theta')Q(r', z, \theta')\ . \tag{18}$$

In the equation above, $\alpha_0 = 2$, while $\alpha_k = 1$ for $k \geq 1$; it is not necessary to specify the coefficients of the terms in $\sin(k\theta)$, since we fix the coordinate system such that $\theta = 0$ at our location, and we are only interested in computing fluxes for this value of θ. Inserting the two expansions in equation (8), we can derive the equation relevant for the propagation in the z direction:

$$\frac{\partial}{\partial z}\,D(z)\,\frac{\partial}{\partial z}\,M_s^k(z) - D(z)\left(\frac{v_s^k}{R_h}\right)^2 M_s^k(z) - \frac{\partial}{\partial z}\,[u(z)M_s^k(z)] - p(z)M_s^k(z) + Q_s^k(z) = 0\ . \tag{19}$$

The solution of this equation is straightforward; it can be easily derived by writing a solution separately for $h_g < z < h_h$, $-h_g < z < h_g$, and $-h_h < z < -h_g$, and then imposing the boundary conditions at $z = \pm h_h$, i.e., equation (15), and the continuity of the number density and of the flux, that is, of $M_s^k(z)$ and $-[D(z)\partial/\partial z]M_s^k(z) + u(z)M_s^k(z)$, at $z = \pm h_g$. For $-h_g \leq z \leq h_g$, the solution is given by

$$M_s^k(z) = M_s^k(0)\cosh(\lambda_g^{ks} z) - \frac{1}{D_g \lambda_g^{ks}} \int_0^z dz' \sinh[\lambda_g^{ks}(z - z')] Q_s^k(z') , \tag{20}$$

where

$$M_s^k(0) = \frac{1}{\cosh(\lambda_g^{ks} h_g)} \left(\frac{I_H}{\sinh[\lambda_h^{ks}(h_h - h_g)]} + \frac{D_h I_{GS}}{D_g \lambda_g^{ks}} \{\gamma_h + \lambda_h^{ks} \coth[\lambda_h^{ks}(h_h - h_g)]\} + I_{GC} \right)$$
$$\times \{D_g \lambda_g^{ks} \tanh(\lambda_g^{ks} h_g) + D_h \gamma_h + D_h \lambda_h^{ks} \coth[\lambda_h^{ks}(h_h - h_g)]\}^{-1} \tag{21}$$

and we have introduced the following set of definitions:

$$\lambda_g^{ks} = \sqrt{\left(\frac{v_s^k}{R_h}\right)^2 + \frac{n_g^{\rm H} v \sigma_{{\rm cr}\,p}^{\rm in}}{D_g}} , \qquad \lambda_h^{ks} = \sqrt{\left(\frac{v_s^k}{R_h}\right)^2 + \frac{n_h^{\rm H} v \sigma_{{\rm cr}\,p}^{\rm in}}{D_h} + \gamma_h^2} , \qquad \gamma_h = \frac{u_h}{2D_h} \tag{22}$$

and

$$I_H = \int_{h_g}^{h_h} dz' \sinh[\lambda_h^{ks}(h_h - z')] \exp[\gamma_h(h_g - z')] \frac{Q_s^k(z') + Q_s^k(-z')}{2}$$
$$I_{GS} = \int_0^{h_g} dz' \sinh[\lambda_g^{ks}(h_g - z')] \frac{Q_s^k(z') + Q_s^k(-z')}{2}$$
$$I_{GC} = \int_0^{h_g} dz' \cosh[\lambda_g^{ks}(h_g - z')] \frac{Q_s^k(z') + Q_s^k(-z')}{2} . \tag{23}$$

For $|z| > h_g$ the solution is analogous but less compact, and it will not be reproduced here. It is more useful to give explicitly $M_s^k(0)$ in case of a source that is constant in the disk and negligible in the halo; in this case,

$$M_s^k(0) = \frac{1}{D_g \lambda_g^{ks2}} \left(1 - \frac{D_h\{\gamma_h + \lambda_h^{ks} \coth[\lambda_h^{ks}(h_h - h_g)]\}}{D_g \lambda_g^{ks} \sinh(\lambda_g^{ks} h_g) + D_h \cosh(\lambda_g^{ks} h_g)\{\gamma_h + \lambda_h^{ks} \coth[\lambda_h^{ks}(h_h - h_g)]\}}\right) Q_s^k(0)$$
$$\equiv M^*(s, k) Q_s^k(0) . \tag{24}$$

It is easy to check that in the limit $u_h \to 0$, equation (24) correctly reduces to the result quoted in Berezinskii et al. (1990, Ch. 3, § 3). Equation (21) also corresponds to the number density found in Chardonnet et al. (1996) and Bottino et al. (1998) in the limits $h_g \to 0$, $D_h \to D_g$, $u_h \to 0$ and for a source function symmetric with respect to the z axis.

Before applying these results to compute cosmic-ray antiproton fluxes, let us pause for a moment. Most commonly, data on cosmic rays have been treated within the framework of the leaky-box approximation. This is, to a certain extent, a simplified version of the diffusion model, where it is assumed that diffusion takes place rapidly. As was noticed, for instance, in Berezinskii et al. (1990), the path length distribution function of particles for a diffusion model with sources in the disk is very close to the exponential form characteristic of the leaky-box treatment. For the purpose of computing secondary antiprotons, which are mainly generated in the gaseous disk, we expect it to be essentially equivalent to write a diffusion equation and fit its parameters to existing data on cosmic-ray nuclei, or to derive from the same data in the simple leaky-box scenario the grammage as a function of rigidity and use it to compute the secondary antiproton flux.

In this sense, we do expect to find an antiproton secondary spectrum that is analogous to the results of several papers in which this has been calculated in the leaky-box approximation (except that in some of these papers not all the relevant effects have been included). On the other hand, in the case of neutralino sources, which are more homogeneously distributed extending through the full halo, it is unlikely that the effective average matter density that particles have gone through can be of the same form as for sources located only in the disk. We will try to analyze in some detail this dependence on the geometry of the source, and we believe that this will give a real improvement with respect to the leaky-box approximation.

5. SOLAR MODULATION

A further complication when comparing predictions of a theoretical model with data on cosmic rays taken at Earth is given by the solar modulation effect. During their propagation from the interstellar medium through the solar system, charged particles are affected by the solar wind and tend to lose energy. The net result of the modulation is a shift in energy between the interstellar spectrum and the spectrum at the Earth and a substantial depletion of particles with nonrelativistic energies.

The simplest way to describe the phenomenon is the analytical force-field approximation of Gleeson & Axford (1967, 1968) for a spherically symmetric model. The prescription of this effective treatment is that, given an interstellar flux at the heliospheric boundary, $d\Phi_b/dT_b$, the flux at the Earth is related to it by

$$\frac{d\Phi_\oplus}{dT_\oplus}(T_\oplus) = \frac{p_\oplus^2}{p_b^2} \frac{d\Phi_b}{dT_b}(T_b) , \tag{25}$$

where the energy at the heliospheric boundary is given by

$$E_b = E_\oplus + |Ze|\,\phi_F\,, \tag{26}$$

and $p_\oplus$ and p_b are the momenta at the Earth and the heliospheric boundary, respectively. Here e is the absolute value of the electron charge and Z is the particle charge in units of e (e.g., $Z = -1$ for antiprotons).

An alternative approach is to solve numerically the propagation equation of the spherically symmetric model (Fisk 1971); the solar modulation parameter one must introduce with this method roughly corresponds to ϕ_F, as given above. When computing solar-modulated antiproton fluxes, the two treatments seem not to be completely equivalent in the low-energy regime (the reader may check, for instance, Fig. 4 in Labrador & Mewaldt 1997 against Fig. 8 in Bottino et al. 1998); keeping this in mind, we will nevertheless implement the force-field approximation, avoiding the problem of having to solve a partial differential equation for each of our supersymmetric models.

We just mention here that the picture can be much more complicated; nonspherical propagation models that take into account the polarity of the solar magnetic field have been studied as well (e.g., Webber & Potgieter 1989). In this case, the solar modulation effects on particles and antiparticles can be quite different. If one would translate this into the force-field effective treatment, one should use different values for the modulation parameter for protons and antiprotons (in contrast to the standard procedure of assigning to antiprotons the value found from proton flux measurements). The relation between these two would be very model dependent.

To compare with the two sets of BESS measurements, which are both near solar minimum, we choose $\phi_F = 500$ MV, in reasonable agreement with what the BESS collaboration uses in their analysis. Otherwise, we will focus on the interstellar fluxes, which are not affected by these uncertainties.

6. BACKGROUND ESTIMATES

6.1. *General Considerations*

Secondary antiprotons are produced in cosmic-ray collisions with the interstellar gas. Looking at the composition of incident and target particles, it is easy to guess that the main contribution to the $\bar{p}$ flux is given by cosmic-ray protons colliding with interstellar hydrogen atoms. Because of baryon number conservation, the minimal $p + p \to \bar{p} + X$ reaction has three protons in the final state; in the rest frame of the target hydrogen atom, the energy threshold for an incident proton to produce an antiproton is therefore $E_p = 7m_p$. Because of this feature, the energy distribution of the produced $\bar{p}$ shows a sharp peak at a few GeV and a steep falloff at lower energies. It is reasonable to expect that in this low-energy region reactions involving heavier nuclei, both as targets and projectiles, may play some role: they imply, in fact, different kinematics, and the spectrum of the produced $\bar{p}$ need not fall as fast as for low-energy pp collisions. We have verified that the interaction of primary protons with interstellar helium is indeed a relevant process, while all others can be safely neglected, since their contributions add up to below a few percent of the total at any energy (this is essentially the same conclusion as reached by Simon, Molnar, & Roesler 1998, although our approach is slightly different, as we point out below). We assume, therefore, that the source function for secondary antiprotons has the following form (the factor of 2 accounts for antiprotons produced by antineutron decays):

$$Q_{\bar{p}}(\boldsymbol{x}, E) = 2\left\{4\pi \int_{E_{\rm thresh}}^{\infty} dE' \left[\frac{d\sigma_{p\,\mathrm{H}\to\bar{p}}}{dE}(E, E')n^{\mathrm{H}}(\boldsymbol{x}) + \frac{d\sigma_{p\,\mathrm{He}\to\bar{p}}}{dE}(E, E')n^{\mathrm{He}}(\boldsymbol{x})\right]\Phi_p(\boldsymbol{x}, E')\right\}. \tag{27}$$

In this formula, $\Phi_p(\boldsymbol{x}, E')$ is the primary proton cosmic-ray flux at the position $\boldsymbol{x}$ in the Galaxy and for the energy E', n^{He} is the helium number density, which we assume to be 7% of n^{H} (Garcia-Munoz et al. 1987) and to have the same spatial dependence, while $d\sigma/dE\,(E, E')$ stands for the differential cross section for the production of an antiproton with energy E for an incident proton of energy E' in the two processes considered. For p-H collisions, we implement the standard parametrization for the differential cross section introduced in Tan & Ng (1983); as already mentioned, the energy threshold ($E_{\rm thresh}$) for this process is $E' = 7m_p$.

6.2. *Antiproton Production in Collisions with Nuclei*

A much smaller set of data is available in the case of antiproton production in proton collisions with heavier elements. In particular, it is difficult to estimate the effects of production below the nominal energy threshold for $p + p \to \bar{p} + X$, which is known to occur in hadron-nucleus collisions. Recently, several experiments have shown substantial subthreshold $\bar{p}$ production for deuterium, helium, carbon, and copper targets (Chiba et al. 1993; Schröter et al. 1993, 1994). Possible collective effects allow the abundant low-energy cosmic rays to produce antiprotons below threshold. On their way out of the nucleus, the produced antiprotons may also suffer inelastic losses which slow them down, creating a potentially important component in the low-energy cosmic-ray–induced $\bar{p}$ spectrum. (Note that helium and heavier nuclei in the cosmic rays also give different kinematics for produced antiprotons. However, this gives an extra contribution at higher $\bar{p}$ energies, and is therefore not important for our study.) These subthreshold effects have been modeled by Sibirtsev et al. (1997), where the limited data set available can be described by a transport equation solved by a Monte Carlo technique.

Here we follow a much simplified approach, which describes the C and Cu data displayed in Sibirtsev et al. (1997) reasonably well and which we apply to $p + \mathrm{He} \to \bar{p} + X$. We find that the collective effects can be mimicked by a shift in the incident proton energy,

$$E_{\rm in} \to E_{\rm eff} = E_{\rm in} + 0.6(E_{\rm thresh} - E_{\rm in})\theta(E_{\rm thresh} - E_{\rm in}) + 1.1\ \mathrm{GeV}\,, \tag{28}$$

where $E_{\rm thresh}$ is the nominal threshold ($7m_p$) for $\bar{p}$ production in pp collisions. The energy loss due to inelastic rescattering can be approximated by decreasing the energy of the outgoing antiproton (using pp kinematics) by 1 GeV. The yield of antiprotons per collision is taken to scale with the total pA cross section, parameterized according to Letaw, Silberberg, & Tsao 1983. In this way, we have a parameterization that is asymptotically correct at high energies and that also fits the subthreshold data. However, we are unable to assess the accuracy of this treatment for the problem at hand; we believe it to be at the 50% level, but acknowledge the need for improved data and theoretical modeling of this seldom-discussed problem.

6.3. *Primary Proton Flux*

The last step to make before implementing equation (27) is to determine the primary proton flux, $\Phi_p(\boldsymbol{x}, E')$. The formalism introduced in § 4 is suitable for this purpose once we specify the source function for primary protons. It is generally believed that supernova remnants are the main sources of cosmic rays. Nevertheless, the gradient of Φ_p as a function of the distance from the Galactic center obtained from the observed distribution of supernovae or the related pulsar distribution is not consistent with models for gamma-ray emission (see Strong & Moskalenko 1998 and references therein). We take advantage of the phenomenological approach of Strong & Moskalenko 1998, in which a generic form for the radial distribution of cosmic-ray sources was considered and its parameters fitted to EGRET gamma-ray data (eq. [6] and Fig. 12 in Strong & Moskalenko 1998). We therefore assume that the primary proton source, in cylindrical coordinates, is of the form

$$Q_p(E, \boldsymbol{x}) = \tilde{q}(E)q(\boldsymbol{x}) = \tilde{q}(E)\left(\frac{r}{r_0}\right)^{0.5} \exp\left(-\frac{r - r_0}{r_0}\right)\theta(h_g - |z|)\,, \tag{29}$$

where $r_0 = 8.5$ kpc is our Galactocentric distance and we have assumed that the energy spectrum of emitted protons is the same everywhere in the Galaxy. The function $\tilde{q}(E)$, which we may interpret as a normalization factor, can be rewritten, after propagation, in terms of the local proton flux, $\Phi_p(r_0, E)$, which has been measured in several experiments. It was argued in the past that the spread among different experimental determinations of $\Phi_p(r_0, E)$ introduces one of the main factors of uncertainty in the prediction for the secondary antiproton flux (see, e.g., Gaisser & Schaefer 1992). The recent measurements by the IMAX (Menn et al. 1997) and CAPRICE (Boezio et al. 1999) collaborations are in better agreement with each other. In Bottino et al. (1998), a fit of the data of these two experiments with a single power law in energy or rigidity was made, using the force-field method to take solar modulation into account. The fits in rigidity (see also Boezio et al. 1999) show a steeper falloff than those in energy; however, this may not be the case if a break in the spectrum at low rigidities is assumed instead (Ormes & Protheroe 1983). As in the next section, the background at high energies will be important, and we prefer to conservatively consider fits with a power law in energy. From equation (1) and Table 1 of Bottino et al. (1998),

$$\Phi_p(r_0, E) = A\,\frac{\sqrt{E^2 - m_p^2}}{E}\left(\frac{E}{1\ \text{GeV}}\right)^{-\alpha}\,, \tag{30}$$

with $A = 12300 \pm 3000$ and $\alpha = 2.67 \pm 0.06$ for the IMAX data, and $A = 19600 \pm 3000$ and $\alpha = 2.85 \pm 0.04$ for the CAPRICE data.

6.4. *Interstellar Secondary Antiproton Flux*

We are now ready to give the formula for the interstellar secondary antiproton flux at our Galactocentric distance. We find

$$\begin{aligned}\Phi_{\bar{p}}(r_0, E) &= \frac{1}{4\pi}\, v_{\bar{p}}(E) N_{\bar{p}}(r_0, E) \\ &= 2v_{\bar{p}}(E)\sum_{s=1}^{\infty} J_0\left(v_s^0\,\frac{r_0}{R_h}\right) M_{\bar{p}}(s, E) I_R(s) \int_{E_{\rm thresh}}^{\infty} dE'\,\frac{(d\sigma_i/dE)(E, E') n^i \Phi_p(r_0, E') M_p(s, E')}{\sum_{s'=1}^{\infty} J_0(v_{s'}^0(r_0/R_h)) M_p(s', E') I_R(s')}\,,\end{aligned} \tag{31}$$

where the repeated index i stands for the sum over hydrogen and helium, and we have introduced the notation

$$I_R(s) = \frac{2}{R_h^2 J_1^2(v_s^0)} \int_0^{R_h} dr'\, r' J_0\left(v_s^0\,\frac{r'}{R_h}\right) q(r') \tag{32}$$

and $M_p(s, E) = M^*(s, k = 0)$, setting the total inelastic cross section appropriate for pp collisions $\sigma_{\text{cr-}p}^{\rm in} = \sigma_{pp}^{\rm in}$, while $M_{\bar{p}}(s, E) = M^*(s, k = 0)$ with $\sigma_{\text{cr-}p}^{\rm in} = \sigma_{\bar{p}p}^{\rm in}$. The parameterizations for both of these cross sections were given in Tan & Ng (1982) as

$$\sigma_{pp}^{\rm in}(T) = \begin{cases} \dfrac{32.2[1 + 0.0273 \ln(E/200)]}{[1 + 0.00262T^{-(17.9 + 13.8 \ln T + 4.41 \ln^2 T)}]}\ \text{mb}, & 0.3 \le T < 3\ \text{GeV} \\ 32.2[1 + 0.0273 \ln(E/200)]\ \text{mb}, & 3 \le T < 200\ \text{GeV} \\ 32.2[1 + 0.0273 \ln(E/200) + 0.01[\ln(E/200)]^2]\ \text{mb}, & T \ge 200\ \text{GeV} \end{cases} \tag{33}$$

and

$$\sigma_{\bar{p}p}^{\rm in}(T) = 24.7(1 + 0.584T^{-0.115} + 0.856T^{-0.566})\ \text{mb}, \quad T \ge 0.05\ \text{GeV}\,, \tag{34}$$

where T and E are in units of GeV. To derive equation (31), we have assumed that for $z < h_g$ the approximation $\Phi_p(z) \simeq \Phi_p(z = 0)$ is valid. This is generally a very good approximation, since for most choices of the parameters in the propagation

model Φ_p is nearly constant in the disk and rapidly decreasing in the halo (see, e.g., Fig. 3.10 of Berezinskii et al. 1990). Only in extreme cases can $\Phi_p(z = h_g)$ be 10% lower than $\Phi_p(z = 0)$, and the correction to the result in equation (31), always below a few percent, can be obtained by keeping track of the full z dependence in J_p (use eqs. [20] and [21]; all numerical integrals in eq. [23] can still be performed analytically, and the result follows easily).

In Bottino et al. (1998), it was suggested that it is a good approximation to assume that the energy spectrum for the protons *after propagation* is roughly independent of location in the Galaxy. This hypothesis simplifies the computation (for us, it is especially needed to compute numerically the tertiary contribution described below); equation (31) then reduces to

$$\Phi_{\bar{p}}(r_0, E) = \frac{2v_{\bar{p}}(E)\int_{E_{\rm thresh}}^{\infty} dE'\,(d\sigma_i/dE)(E, E')n^i\Phi_p(r_0, E')}{\sum_{s'=1}^{\infty} J_0[v_{s'}^0(r_0/R_h)]M_p(s', \hat{E})I_R(s')} \sum_{s=1}^{\infty} J_0\left(v_s^0 \frac{r_0}{R_h}\right) M_{\bar{p}}(s, E)M_p(s, \hat{E})I_R(s)\,, \tag{35}$$

where $\hat{E}$ is an arbitrary normalization energy. Since there are some indications that the energy spectrum may indeed be steeper far away from the sources, because of the energy dependence in the propagation coefficient (Mori 1997), we compare in one case equation (35) against equation (31) to check whether the simplification in any way changes the result. For the set of parameters as in the example in Figure 1, which we discuss below, we find that equation (35) gives a very slight overestimate of equation (31), below 3% for interstellar antiproton kinetic energies up to 1 GeV, a maximal 5.5% overestimate at 3 GeV, while for higher energies the difference decreases again and is below 4% at 50 GeV (we remark, however, that we have not tuned our propagation model to reproduce the effect in Mori [1997], so we cannot claim that this effect is not relevant).

6.5. *Tertiary Antiprotons*

In equation (8) we have not introduced any energy-changing term. We now include energy losses for secondary antiprotons due to scattering processes during their propagation in the Galaxy. The main effect is due to nonannihilation inelastic interactions of antiprotons with interstellar protons, giving lower energy antiprotons in the final state. Actually, the energy distribution after the nonannihilation interaction is not well known, since there are no direct measurements; the usual assumption (Tan & Ng 1982) is that the distribution is similar to the final-state proton in pp inelastic (nondiffractive) interactions, i.e., a rather flat distribution in kinetic energy between zero and the kinetic energy of the incident antiproton. One might think that elastic scattering processes are relevant as well, but available data show that the cross section is dominated by the forward peak with very small energy transfer (Eisenhandler et al. 1976; Brückner et al. 1986), and hence with a marginal net effect from our point of view. We therefore include only nonannihilation processes, considering a "tertiary" source function generated by inelastically scattered secondary antiprotons, in the form

$$Q_{\bar{p}}^{\rm tert}(\boldsymbol{x}, E) = 4\pi n^{\rm H}(\boldsymbol{x})\left[\int_E^{\infty} \frac{\sigma_{\bar{p}p}^{\rm nonann}(E')}{T'} I_{\bar{p}}(\boldsymbol{x}, E')dE' - \sigma_{\bar{p}p}^{\rm nonann}(E)I_{\bar{p}}(\boldsymbol{x}, E)\right], \tag{36}$$

where $\sigma_{\bar{p}p}^{\rm nonann}$ is obtained as the difference between the total inelastic cross section equation (34) and the inelastic annihilation cross section,

$$\sigma_{\bar{p}p}^{\rm ann}(T) = \begin{cases} 661(1 + 0.0115T^{-0.774} - 0.948T^{0.0151})\ {\rm mb}, & T < 15.5\ {\rm GeV} \\ 36T^{-0.5}\ {\rm mb}, & T \geq 15.5\ {\rm GeV}\,, \end{cases} \tag{37}$$

where for lower energies we have used the parametrization from Tan & Ng (1982), while in the high-energy range we apply the approximation given in Protheroe (1981). Both this parametrization and those needed above have been checked against a compilation of more recent data (Caso et al. 1998). The second term in equation (36) takes into account antiprotons that are depleted from the energy E and which we propagate as a negative flux; it actually gives an effect that is less than a few percent at any energy and is not needed in our formalism. As was done for equation (27), it is straightforward to write a Fourier-Bessel expansion for $Q_{\bar{p}}^{\rm tert}$ and then compute $\Phi_{\bar{p}}^{\rm tert}$, which must be summed to $\Phi_{\bar{p}}$ to get the final expression for the background interstellar antiproton flux.

6.6. *Numerical Results*

Coming to the actual numerical predictions for the background flux of antiprotons, we base our choice of parameters on the propagation model from previous work in which diffusion models analogous to the one described in § 4 were used to fit data on cosmic-ray nuclei, such as ratios of secondaries to primaries and of radioactive nuclei to their stable counterparts. Actually, slightly discrepant results are present in the literature, partly reflecting the fact that it is not easy to find a propagation model that is consistent with the whole set of existing data. We consider three different scenarios here and in the following section when describing the signal from neutralino annihilations. We only keep the following parameters fixed: $n_g^{\rm H} = 1\ {\rm cm}^{-3}$, $n_h^{\rm H} = 0$, $h_g = 0.1$ kpc, and $R_h = 20$ kpc. The first three are the standard values inferred from direct observation. The last one, which in the literature is taken sometimes as small as 15 kpc, and which in Strong & Moskalenko (1998) is set equal to 30 kpc, does not play a major role, and different choices lead to nearly equivalent results.

The three scenarios are:

1. In the case of $D_g^0 = D_h^0 = D^0$, our propagation model is fairly close to the one considered by Webber et al. (1992). Their conclusion is that a thin halo is preferred, with height $h_h \in (1.1,3.8)$ kpc and $D \simeq (6 \pm 4) \times 10^{27}\ {\rm cm}^2\ {\rm s}^{-1}$ at the rigidity $R = 1$ GV. The flux shown in Figure 1 is obtained in this scenario, setting $h_h = 3$ kpc, $D^0 = 6 \times 10^{27}\ {\rm cm}^2\ {\rm s}^{-1}$, and $R_0 = 3$ GV, choosing the proton flux at the Earth as the medium value in the fit of IMAX data, i.e., with $A = 12{,}300$ and $\alpha = 2.67$, and taking into account solar modulation with the force-field method with $\phi_F = 500$ MV, as suggested by the analysis of the BESS

collaboration. There is no consensus in the literature on the value of the solar modulation parameter at solar minimum; nevertheless, the spectrum does not change dramatically if a slightly different value for ϕ_F is assumed. For instance, $\phi_F = 400$ MV gives about a 7% increase at the kinetic energy $T = 0.2$ GeV, and about an 8% increase at the maximum. For $\phi_F = 600$ MV the effect is reversed, and we find that the flux is lower by roughly the same percentages as in the previous case.

As will become clear in the following discussion, the background antiproton flux shown in Figure 1 is only an example of the possibility of a good fit to the data; we keep it as reference case to compare with. In Figure 3, we show for the same parameters the interstellar antiproton flux versus kinetic energy T, plotting also its three main components: the secondary antiproton flux due to *pp* collisions, the contribution from *p*He scattering processes, and the tertiary component due to energy loss. As can be seen, the first contribution is dominant at the maximum and at high energies, while the other two are important in the low-energy region.

We take advantage of Figure 3 to show another feature that is common for all choices of the propagation parameters, the uncertainty due to the interstellar proton flux. The band around our reference antiproton flux is the envelope of the predictions obtained by using the uncertainty in the proton flux (Bottino et al. 1998); the upper bound is given choosing the fit of IMAX data with $A = 15{,}300$ and $\alpha = 2.61$ (average values $+1\ \sigma$ and $-1\ \sigma$, respectively), while the lower bound below $T = 2.5$ GeV is obtained from the IMAX data fitted with $A = 9300$ and $\alpha = 2.73$, and above 2.5 GeV from the CAPRICE data fitted with $A = 16{,}300$ and $\alpha = 2.89$ (average values $-1\ \sigma$ and $+1\ \sigma$, respectively; in fact, these two spectra are nearly overlapping at all energies).

Coming back to the uncertainty in the choice of the propagation parameters in the Webber-Lee-Gupta scenario, if we now pick the average value for the halo height as $h_h = 2$ kpc, and vary the diffusion coefficient in the suggested interval $D^0 \simeq (3\text{–}7) \times 10^{27}$ cm^2 s^{-1} for $R_0 = 3$ GV, we find that the flux at intermediate energies increases by up to about 30% for the smallest value of the diffusion coefficient, while it decreases with a slightly higher percentage for the highest value of D^0. This is represented by the band in Figure 4*a* [both in this figure and in Fig. 6 below, we define fractional differences as $(\Phi - \Phi_R)/\Phi_R$, where Φ_R is the reference value, i.e., in this case the flux shown as a solid line in Fig. 3]. If we assume, on the other hand, that D^0 and h_h are linearly related, a degeneracy that may indeed not be resolved by available data, and fix $D^0 = 2.5(h_h/\text{kpc}) \times 10^{27}$ cm^2 s^{-1}, varying h_h between 1.1 and 3.8 kpc, we get a band of very small width, below a few percent (Fig. 4*a*, *solid and dashed lines at about* -20%).

2. In Strong & Moskalenko (1998), a scenario is favored with a thicker halo, with $h_h \in (4,12)$ kpc, when no convection is assumed. Their treatment of propagation is not as close to our model as the previous case, so the way we translate their typical choice of parameters into our picture is less safe, but it should give at least the right qualitative behavior. We sketch the thick-halo scenario taking $h_h \in (4,12)$ kpc, $D_h^0 = 2.5(h_h/\text{kpc}) \times 10^{27}$ cm^2 s^{-1}, $D_g^0 = 6 \times 10^{27}$ cm^2 s^{-1}, and $R_0 = 1$ GV, a choice consistent with the results of Ginzburg et al. (1980), where the propagation model we have chosen was first considered. Comparing to our reference case, we find a band of 20% width around an average suppression of the flux of about 50%, where the least severe suppression is given by the smallest halo considered, and the maximal suppression corresponds to the large halo $h_h = 12$ kpc (Fig. 4*b*, *solid and dashed lines, respectively*).

3. As a third scenario, we allow for the presence of a Galactic wind driving cosmic rays out of the Galactic disk. Self-consistent models for the propagation of cosmic rays in magnetohydrodynamic flows have been studied recently in detail (Zirakashvili et al. 1996; Ptuskin et al. 1997). The much simpler approach we take here is intended to compare qualitatively the effects of the wind on the background antiproton flux and on the signal from neutralino annihilations. Considering again the model in the previous scenario with $h_h = 4$ kpc (Fig. 4*c*, *solid curve*), we take as an example the case of $v_h = 10$ km s^{-1}

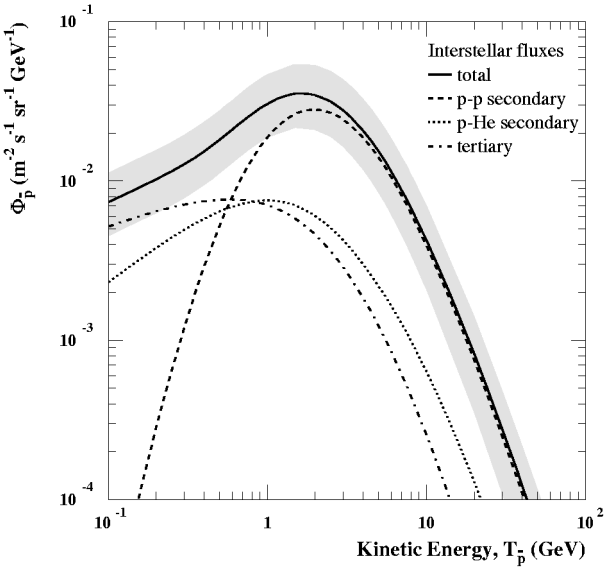

FIG. 3.—Interstellar antiproton flux and the contribution from secondary and tertiary antiprotons. The uncertainty due to the parametrization of the primary proton spectrum is also shown by the shaded band. The solid line corresponds to the same set of parameters as in Fig. 1.

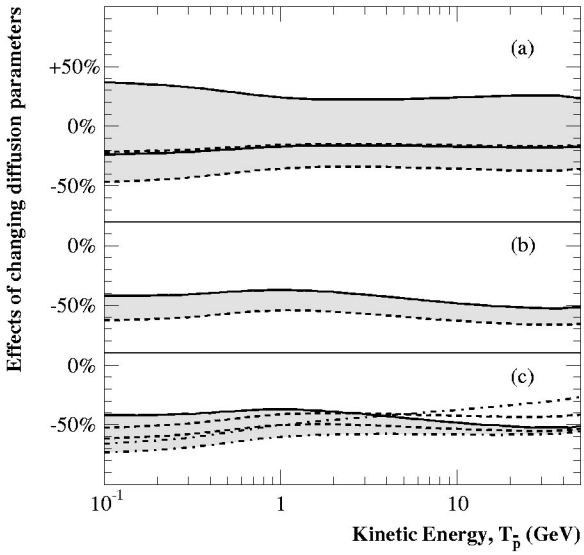

FIG. 4.—Effects of changing the diffusion parameters are shown for (*a*) the thin halo scenario, (*b*) the thick halo scenario, and (*c*) a convective halo. See text for further details.

(*lower dashed line*) and $v_h = 20$ km s^{-1} (*lower dash-dotted line*). As can be seen, in perfect analogy with the case of the solar wind, the Galactic wind alters the spectrum at low energies (up to 30% in the example we are considering), while the effect gets smaller and smaller for more energetic particles. If in analogy with the parameter choice of Strong & Moskalenko we suppose that there is some scaling between v_h and D_h^0, for instance, a simple linear scaling $D_h^0 = 2.5(h_h/\mathrm{kpc})[(40 \text{ km s}^{-1} - v_h)/40 \text{ km s}^{-1}] \times 10^{27}$ cm^2 s^{-1}, we find that at intermediate energies the flux is nearly unchanged (Fig. 4*c*, *upper dashed and dash-dotted lines*).

We will not combine the uncertainty bands we have just derived and make a definite statement about the uncertainty on the prediction of the cosmic antiproton background. To be able to do that on a firmer basis, we should compare the predictions of our propagation model directly against the whole set of data on cosmic-ray nuclei, and this is beyond the aim of the paper. We stress again that this section was mainly intended to show that the most recent data on cosmic-ray antiprotons can be fitted by the background flux for some natural choice of the diffusion parameters. On the other hand, we find that the prediction for the background could be lower as well, leaving room for an antiproton flux generated by an exotic source, possibly dark matter neutralinos.

6.7. *Reacceleration*

It seems very plausible that cosmic rays are reaccelerated by a Fermi type of acceleration by stochastic magnetic fields during propagation. This has been discussed in, e.g., Seo & Ptuskin (1994), Heinbach & Simon (1995), and Simon & Heinbach (1996). There is also a possibility that cosmic rays get reaccelerated by weak shock waves from supernova remnants (Letaw et al. 1993). We will here focus on the former process, usually called diffusive reacceleration since it can be treated as a diffusion in momentum space.

In Heinbach & Simon (1995), it was shown that data on low-energy cosmic rays are compatible with the predictions of models without diffusive reacceleration only if the mean path length variation with energy shows a sharp break around 1–2 GeV. In models that include reacceleration effects, on the other hand, depending on reacceleration strength, a path length distribution that is a simple power law for all energies may be considered. This is theoretically appealing, since this form derived from observations agrees well with that expected from Kolmogorov turbulence. The result of Heinbach & Simon (1995) is confirmed in the analysis by Strong & Moskalenko (1998), who conclude as well that the reacceleration scheme allows a more natural choice for the parameters in the propagation model.

Even though reacceleration implies that the average energy increases as the cosmic rays propagate through the Galaxy, there is a general smearing of the injected spectrum, meaning that there is also a "leakage" of cosmic rays from higher energies to lower.

This might be important for antiprotons where the injected spectrum drops below the maximum at few GeV. In Simon & Heinbach (1996) it was found that this leakage could substantially increase the secondary $\bar{p}$ spectrum below 1 GeV, with a flux at a few hundred MeV that hardly can be lower than $\frac{1}{3}$ of the value at around 1 GeV. We cannot compare directly with our analysis, since we are not applying the same primary proton spectrum and propagation model, but still we can conclude that including reacceleration in the propagation model might add up to the effects of the proton-nuclei interactions and of the tertiary component in flattening the antiproton spectrum at low energies, making it even more problematic to separate an exotic signal from the background in this region of the antiproton spectrum.

7. SIGNAL FROM NEUTRALINO ANNIHILATION

7.1. *General Discussion*

With the source function introduced in equation (6), the antiproton flux from neutralino annihilations in the Galactic halo is readily obtained from the formulas derived in § 4. It is given by

$$\Phi_{\bar{p}}(r_0, T) = \frac{1}{4\pi} v_{\bar{p}}(T) N_{\bar{p}}(r_0, T) = \frac{1}{4\pi} v_{\bar{p}}(T) \sum_{s=1}^{\infty} J_0\left(\nu_s^0 \frac{r_0}{R_h}\right) M_s^0(0) , \tag{38}$$

where $M_s^0(0)$ is obtained from equation (21) with $\sigma_{\mathrm{cr}p}^{\mathrm{in}} = \sigma_{\bar{p}p}^{\mathrm{in}}$ in equation (22) and $Q_s^0(z)$ in equation (23), given by

$$Q_s^0(z) = \frac{2}{R_h^2 J_1^2(\nu_s^0)} \int_0^{R_h} dr' r' J_0\left(\nu_s^0 \frac{r'}{R_h}\right) Q_{\bar{p}}^{\chi}(r', z) . \tag{39}$$

It is possible to separate in the expression for the signal the part that depends on the MSSM parameter space from the terms that are related only to the distribution of sources in the propagation region and to the propagation model itself. We introduce the definition

$$\Phi_{\bar{p}}(r_0, T) \equiv (\sigma_{\mathrm{ann}} v) \sum_f \frac{dN^f}{dT} B^f \left(\frac{\rho_0}{m_{\tilde{\chi}}}\right)^2 C_{\mathrm{prop}}(T) . \tag{40}$$

The quantity C_{prop}, which can be obtained explicitly by comparing equation (38) with equation (40), has the dimension of length divided by solid angle and is analogous to the coefficient defined in equation (46) of Bottino et al. (1998); note, however, that in equation (40) we have factorized the value of the local halo density, ρ_0, rather than some reference density.

7.2. *Uncertainties Related to Propagation*

Having factorized out in equation (40) the dependence of the signal on the choice of the dark matter candidate, we analyze first how sensitive the result is to the set of parameters that define both the location of the sources and the propagation of the produced antiprotons. We fix a reference configuration selecting for the propagation model, in analogy to the analysis of the background flux, the same parameters as in the example in Figures 1 and 3 ($h_h = 3$ kpc, $D^0 = 6 \times 10^{27}$ cm^2 s^{-1}, and $R_0 = 3$ GV), while as a reference dark matter density profile we choose a modified isothermal distribution, equation (7) with $(\alpha, \beta, \gamma) = (2, 2, 0)$ and with an intermediate value for the length scale, $a = 3.5$ kpc. In Figure 5 we plot the value of C_{prop} for this reference case (*solid curve*) versus the antiproton kinetic energy. C_{prop} is increasing in the low-energy range, since it contains the kinematic factor $v_{\bar{p}}(T)$, and at the same time we have assumed that the diffusion coefficient is roughly constant at low rigidities (see eq. [11]). The coefficient C_{prop} then reaches a maximum at about $T \simeq 2$ GeV, while at higher energies it decreases as a consequence of the 0.6 power-law increase in the diffusion coefficient.

First we analyze how the result changes if for the dark matter density distribution we consider the profile from Navarro et al. (1996), which is singular toward the Galactic center, i.e., equation (7) with $(\alpha, \beta, \gamma) = (1, 2, 1)$. Choosing $a = 9$ kpc, we obtain (see Fig. 5, *dotted line*) roughly a 33% increase in C_{prop} (and therefore in the signal from neutralino annihilations) at any T, while the more cuspy profile with $a = 3.5$ kpc gives a result that is more than twice the reference value. This is rather surprising, because even though the singularity in the profile induces a sharp enhancement in the neutralino number density

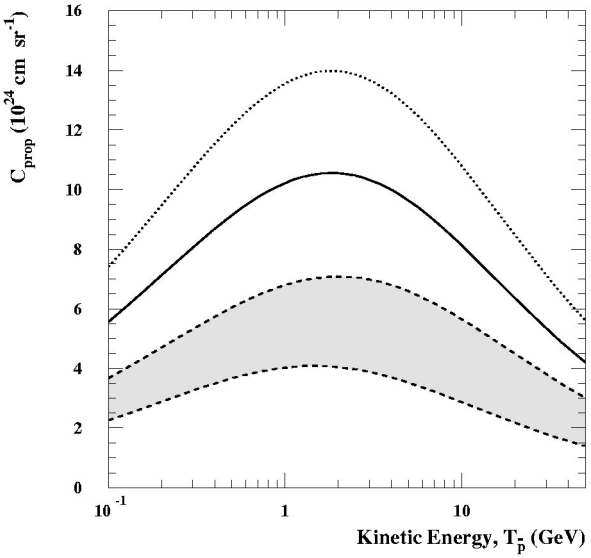

FIG. 5.—Value of C_{prop} for the same choice of diffusion parameters as in Fig. 1 and an isothermal sphere distribution of dark matter with $a = 3.5$ kpc (*solid line*), compared to the value for the same diffusion parameters and a Navarro et al. (1996) profile with $a = 9$ kpc (*dotted line*). The band gives the range of values of C_{prop} in the thin halo scenario (with $h_h = 2$ kpc), as described in the text.

and therefore in the strength of the source, this cusp is at the Galactic center, rather far away from the solar system. It is commonly believed that in the diffusion regime the local sources are the most relevant, but at least in the propagation model we are considering, this is not true: for the Navarro et al. profile with $a = 9$ kpc, 23% of the signal is given by sources contained in a spherical region of 1 kpc around the Galactic center; the percentage increases to 42% for $a = 3.5$ kpc, while it is as low as 1% for the isothermal sphere profile. We conclude that nonlocal sources may give a significant contribution, provided that their strength is much enhanced with respect to the local ones. This effect should be considered in more detail when considering a clumpy scenario (Ullio 1999), for which it may be even more relevant.

Figure 5 contains another piece of information. Going back to the case in which the dark matter density profile is described by an isothermal sphere, we have varied the parameters that define the propagation model, going through the same three scenarios described when discussing the background. The band in the figure is given by fixing $h_h = 2$ kpc and varying the diffusion coefficient in the interval $D^0 \simeq (3\text{–}7) \times 10^{27}$ cm^2 s^{-1}, and corresponds to the band shown in Figure 4*a* (again, the highest value of D^0 gives the lowest value for the flux). Unlike the latter, the band in Figure 5 does not overlap the reference value (*solid line*); for the signal from neutralino annihilations, the decrease in the height of the propagation zone from 3 to 2 kpc is not compensated for by the decrease in the central value for the diffusion coefficient. This gives a first hint of how sensitive the dark matter signal is to the choice of the value of the height of the diffusion zone.

The same effect is studied in the upper part of Figure 6, fixing the kinetic energy to $T = 1$ GeV, varying h_h, and linearly relating D^0 to h_h, as introduced in the previous section. According to the Webber-Lee-Gupta scenario, h_h is constrained to be between 1.1 and 3.8 kpc; the degeneracy we found for the background flux (Fig. 4*a*, *nearly overlapping solid and dashed lines*) is completely removed for the signal from neutralino annihilations, going from an 80% suppression to a 20% increase compared to the reference value for minimal and maximal h_h, respectively. Changing the diffusion zone height modifies the number of sources that contribute to the flux, since sources that are outside the diffusion box are not included in the model. Therefore, it is not surprising that a very thin diffusion zone gives a suppressed signal, while larger values for h_h enhance it.

In the same way, in the thick-halo scenario without convection, inferred from the analysis of Strong & Moskalenko (1998), the suppression band found for the background flux (Fig. 4*b*) becomes a much wider band, for which the signal flux is increased instead (Fig. 6*b*, *solid line*). The enhancement with the diffusion-zone height is flattened out at high values of h_h, since the new sources we include are farther and farther away from the observer, and moreover the density profile falls at large Galactocentric distances.

While the effects we have considered so far give roughly the same result for any value of the antiproton kinetic energy, the effect of convection in the z-direction is clearly energy dependent. In *c1* of Figure 6, we plot $C_{\rm prop}$ as a function of the Galactic wind speed for $h_h = 4$ kpc, $D_h^0 = 10^{28}$ cm^2 s^{-1}, $D_g^0 = 6 \times 10^{27}$ cm^2 s^{-1}, and $R_0 = 1$ GV (we consider here as reference value the one obtained with this set of parameters and $u_h = 0$). In *c2* of Figure 6, as we did for the background, D_h^0 is taken to be

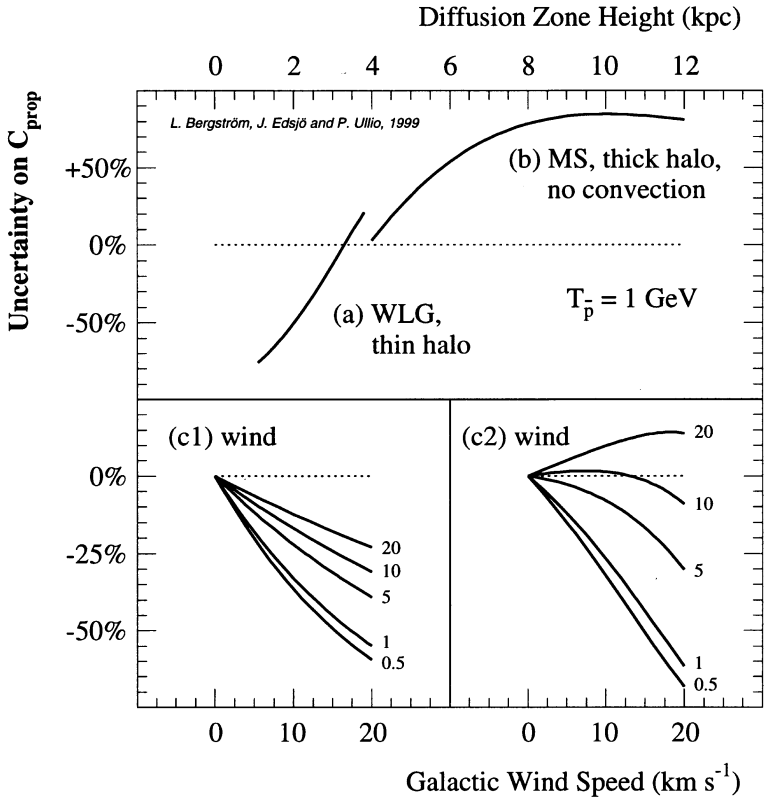

FIG. 6.—Changes of $C_{\rm prop}$ when the diffusion zone height is changed within (*a*) the thin halo scenario derived from the Webber et al. (1992) model and (*b*) the thick halo scenario inspired by the Strong & Moskalenko (1998) analysis. In (*c*) the effects of a convective wind are sketched: in *c1* the diffusion coefficient is kept fixed, while in *c2* it is linearly scaled with the Galactic wind.

related linearly to the value of the wind speed. In both, five different kinetic energies (given in the figure in GeV) have been considered. As can be seen going back to Figure 4*c*, the effect of convection is greater on the signal from neutralino annihilation than on the background flux. Especially at low energies, it is not well compensated for by the linear scaling of the diffusion coefficient.

For the background flux, the effect of introducing a Galactic wind is to drive antiprotons more quickly from the disk, where they are generated, to the border of the diffusion zone, where they are lost. This effect can be balanced by lowering the diffusion coefficient, that is, assuming that diffusion takes place less efficiently. The sources of the signal, on the other hand, are distributed over the whole diffusion box; setting with the Galactic wind a preferred direction of propagation lowers the probability that an antiproton generated relatively far away from the disk will reach our location. The effect is not compensated for by the rescaling of D_h^0, at least not for the rescaling needed for cosmic-ray species generated in the disk.

The last check we perform regards the role played by the antiprotons produced outside the propagation region. Our solution to the diffusion equation has been derived under the hypothesis that the number density of the considered cosmic-ray species is zero at the boundary of the diffusion zone. This is not strictly true for the signal from neutralino annihilations. One possibility for verifying what kind of corrections might be needed in this case is to compare the antiproton flux leaving the diffusion zone with the flux injected by external sources. We restrict the analysis to exchanges at the boundary $z = \pm h_h$, since the effect is much suppressed in the radial direction, being generally $R_h \gg h_h$.

The outgoing flux can be computed by keeping track of the full dependence on z of the number density, since this flux is related to the gradient of the number density at the boundaries; one derives a rather lengthy expression, which we do not reproduce here but which follows in a straightforward way. For the injected flux, we use the very simple picture of propagation in free space, summing contributions over the line of sight. For the modified isothermal sphere profile and a diffusion zone height of 3 kpc, we find that the ingoing flux is about one-third of the outgoing flux for very small radial coordinates, while they become roughly equal at $r = 8$ kpc, and at larger radii the injected flux becomes prevailing; the total number of antiprotons per second that penetrate the diffusion box is about 70% of those that leave it.

As can be understood, this fraction is smaller if we consider instead the Navarro et al. (1996) profile or if we pick a higher value for the diffusion zone height, and might turn into a rather large number for very thin halos. To give a precise numerical estimate for the effect, one should add in the propagation model a third zone above $|z| = h_h$. However, taking into account all the other uncertainties that enter in the prediction for the signal, we do not consider this worthwhile at present. We believe that a safe assumption is that the signal from neutralino annihilations has not been underestimated due to this effect by more that a factor of 2 in the most extreme cases.

7.3. *Antiprotons from Specific MSSM Models*

The antiproton spectra from neutralino annihilations have been calculated for all the different MSSM models given in Table 1. In Figures 7–11 we show our main results. We use our canonical parameters for propagation and the isothermal sphere model for the halo profile.

7.3.1. *Interstellar Fluxes*

In Figure 7*a* we show the predicted interstellar antiproton flux at a kinetic energy of 1 GeV (i.e., without corrections for solar modulation) versus the neutralino mass. We clearly see the trend that the flux goes down with the mass of the neutralino.

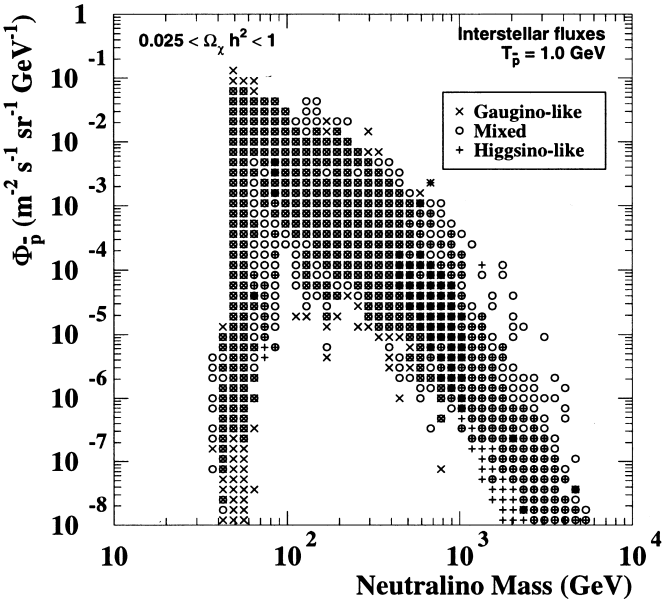

FIG. 7*a*

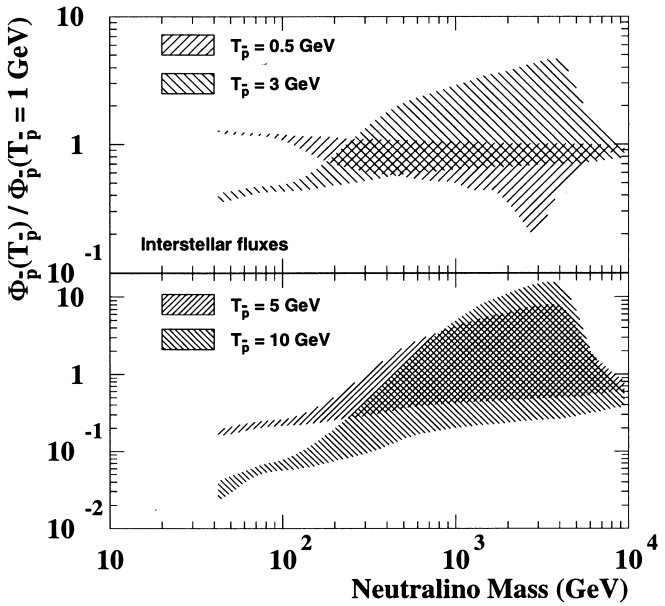

FIG. 7*b*

FIG. 7.—(*a*) Interstellar antiproton flux at 1 GeV. (*b*) Ratio of the flux at different kinetic energies to that at 1 GeV. To make the figure clearer (and avoid showing artifacts of sampling frequency), the figure is binned. We also indicate in which bins there are models that are gaugino-like (*crosses*), mixed (*open circles*), and Higgsino-like (*plus signs*).

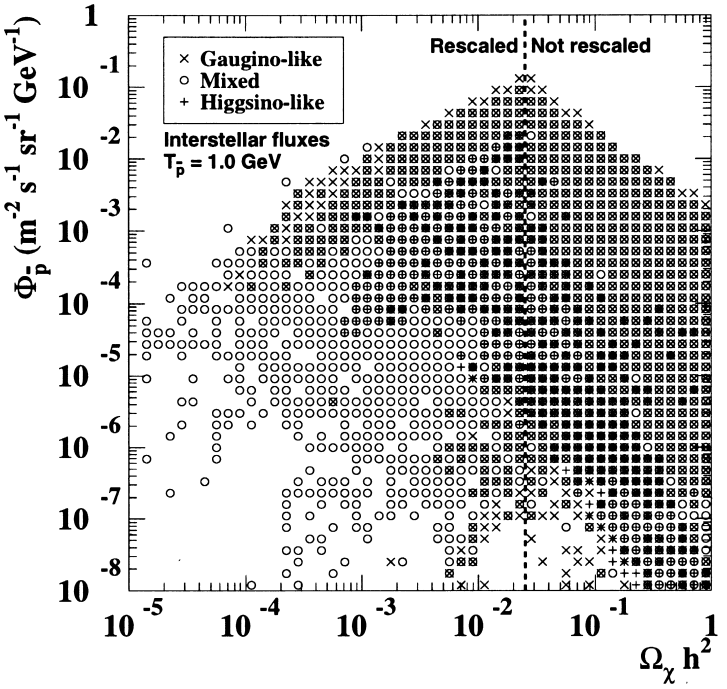

FIG. 8.—Interstellar antiproton flux at 1 GeV vs. the relic density. This is the only figure in which models having $\Omega_\chi h^2 < 0.025$ are shown.

The reason for this is that the number density of neutralinos goes down as the mass increases, for a given interval of the dark matter mass density. Since $n_\chi = \rho_\chi/m_\chi$ and the annihilation rate scales as n_χ^2, the suppression increases rapidly with mass. At the lower mass end, the present accelerator limits preclude a neutralino in the MSSM below a few tens of GeV. The low-flux models at low masses will be discussed in connection with Figure 8 below.

The points in the figure are coded with different symbols for different compositions of the neutralino. We define models with $0 < Z_g < 0.01$ as Higgsino-like, $0.01 < Z_g < 0.99$ as mixed, and $0.99 < Z_g < 1$ as gaugino-like. As can be seen, most of the models with high rates are either gaugino-like or mixed, except at masses greater than several hundred GeV, where

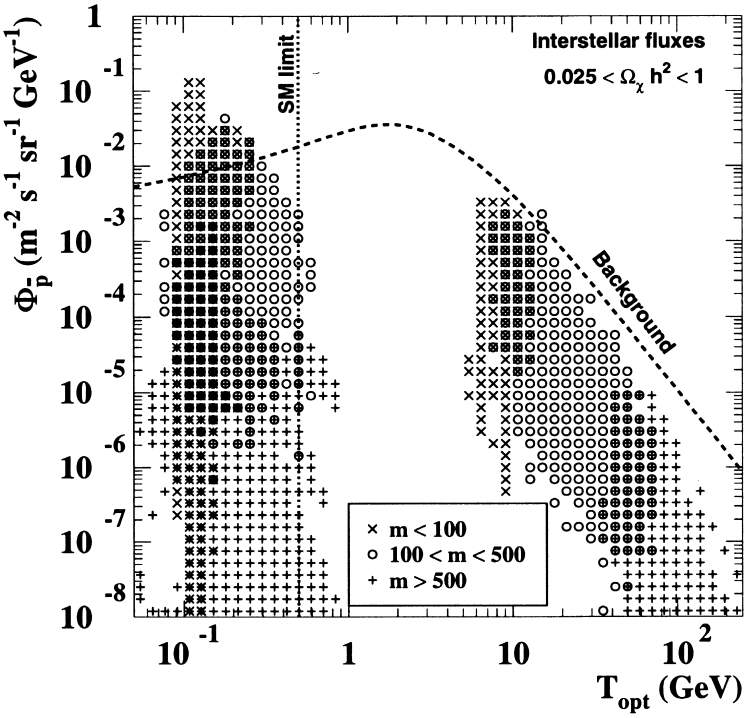

FIG. 9.—Flux of antiprotons from neutralino annihilation at the optimal kinetic energy (T_{opt}) vs. T_{opt}. T_{opt} is defined as the energy at which $\Phi_{signal}/\Phi_{background}$ is highest; if the spectrum has more than one optimum, the highest two have been included in the plot. The models have been coded according to the neutralino mass in GeV.

Higgsino-like models can also be important. (In fact, there is also a small mass window around 80 GeV where Higgsinos may be relevant.)

In Figure 7*b*, we show the ratio of the interstellar flux at 0.5, 3, 5, and 10 GeV to the flux at 1 GeV displayed in Figure 7*a* for the same set of models (but without coding the composition). It can be seen that for the higher mass models, it can be more advantageous to study the flux at higher kinetic energies.

In Figure 8 we show the same fluxes as in Figure 7*a*, but versus the relic density, $\Omega_\chi h^2$. There is a very clear trend that the highest flux is obtained when $\Omega_\chi h^2$ is close to the lowest acceptable relic density. The reason for this is that if the annihilation cross section is increased, the flux of antiprotons increases, but since the relic density $\Omega_\chi h^2$ is approximately inversely proportional to the annihilation cross section, $\Omega_\chi h^2$ decreases, and hence the strong correlation. The correlation is not perfect, however, since it is the thermally averaged cross section at a temperature of about $m_\chi/20$ that determines $\Omega_\chi h^2$, whereas the annihilation in the halo to a very good approximation occurs at rest (the speeds are typically $\sim 0.001c$).

This also explains some features in Figure 7*a*. In the mass range between 40 and 60 GeV there exist models that give exceedingly small rates, but also some that give the highest of all rates. This large spread reflects peculiarities near the Z^0 (and neutral Higgs) resonances and the W^+W^- threshold. For the low-flux models around 40–60 GeV, the annihilation cross section at rest is very small, but either a resonance or a threshold can be reached through thermal motion in the early universe, and the relic density is reduced to our selected range $0.025 < \Omega_\chi h^2 < 1$. As shown by Chen & Kamionkowski (1998),[2] three-body final states can be important (not too far) below the W^+W^- and the $t\bar{t}$ thresholds, and this could enhance the signal for these low-rate models.

We also have some models around 130 GeV that give high fluxes. In this case, it is the other way around; the masses are just so that we are on the H_3^0 resonance for the nonrelativistic speeds in the halo, but the thermal average in the early universe gives a lower annihilation cross section, and hence the relic density is increased to our desired range, $0.025 < \Omega_\chi h^2 < 1$. The behavior at 130 GeV is just accidental; it could happen at any important resonance. In fact, we found only one high-flux model around 130 GeV in our "normal" scans, and we performed a small scan varying the parameters slightly around this model. The relic density was essentially unchanged, but the antiproton flux showed large variations depending on whether we were below, on, or above the resonance.

In Figure 8 we also show models with a value of Ωh^2 lower than our required limit of 0.025. In principle, one could accept these models at the expense of introducing other components of dark matter. To be consistent, one should then rescale the local dark matter density in the form of neutralinos by some unknown factor. In the absence of better procedures, one usually employs a linear rescaling, $\rho_\chi = (\Omega_\chi h^2/0.025)\rho_{\rm DM}$. Since the annihilation rate is quadratic in the number density, this rescaling factor enters squared in the predicted $\bar{p}$ rate, something that is clearly visible in Figure 8.

We are now interested in finding out whether there are any special features of the antiproton spectra from neutralino annihilation that distinguish these spectra from the background. We have already mentioned that the window at low energies may not be as good as previously thought. We will here investigate other features and energy regions of the spectrum to see whether there are good signatures of a neutralino contribution to the flux.

One thing that might differ is the slope at different energies. The background is expected to have a rising trend at low energies, reaching a maximum between 1 and 2 GeV (see Fig. 3) and with a slope of around -3 at high energies. On the other hand, the high-rate models tend to be decreasing at 1 GeV (see Fig. 11*a*). This may cause a shift of the maximum of the summed spectrum (signal plus background) to a lower energy, which is a possible signature.

We next investigate whether there is an optimal energy at which $\Phi_{\rm signal}/\Phi_{\rm background}$ has a maximum (for this purpose we will use the reference background given in Fig. 3). In Figure 9 we show the flux at these optimal energies ($T_{\rm opt}$) versus $T_{\rm opt}$. We now see that we have two classes of models: one class that have the highest signal-to-noise ratio below 0.5 GeV (i.e., inaccessible in the solar system due to the solar modulation), and one that have the highest signal-to-noise ratio at 10–30 GeV. For this first class of models, we note that there exists a proposal for an extrasolar space probe (Wells, Moiseev, & Ormes 1998) that would avoid the solar modulation problem, and is thus an attractive possibility for this field. However, these models have high rates in the range 0.5–1 GeV as well, even though it would be even more advantageous to go to lower energies. The second class of models are much less affected by solar modulation and also give reasonably high fluxes. In Figure 11*a*, below, we show some examples of spectra. All of these have optimal energies in the low-energy region, but, e.g., spectrum 3 has an optimum at high energy as well.

7.3.2. *Solar-modulated Fluxes*

We now turn to the solar-modulated fluxes and will compare our results with the BESS 97 measurements, which we recall are in very good agreement with our estimate for the background flux. We will compare the fluxes in two of the BESS energy bins, the one at 0.35 GeV and the one in which the measured flux is the highest. In Figure 10 we show the solar-modulated fluxes versus the neutralino mass. We see the same general trend as for the interstellar fluxes (Fig. 7), but we also see that there are many models with fluxes above the BESS measurements. However, this conclusion depends strongly on what range one allows for the neutralino relic density. In Figure 10 we have coded the symbols according to the relic density interval. As can be seen, essentially all models that are in the BESS measurement band have a relic density $\Omega_\chi h^2 < 0.1$. If we instead require $0.1 \lesssim \Omega_\chi h^2 \lesssim 0.2$, the rates are never higher than the measured flux.

This points to a weakness of this indirect method of detecting supersymmetric dark matter: once the predicted rate is lower than the presently measured flux, the sensitivity to an exotic component is lost. This is because of the lack of a distinct signature that could differentiate between the signal and the background. Alternative indirect search methods, such as using gamma rays from the halo (see, e.g., Bergström, Ullio, & Buckley 1998b) or neutrinos from the Sun or the Earth (see, e.g.,

[2] The Journal of High-Energy Physics (Chen & Kamionkowski 1998) is available at: http://jhep.mse.jhu.edu.

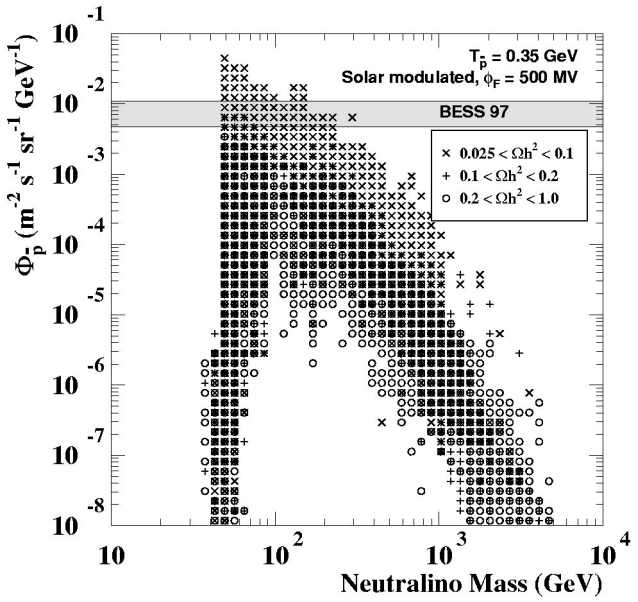

FIG. 10*a*

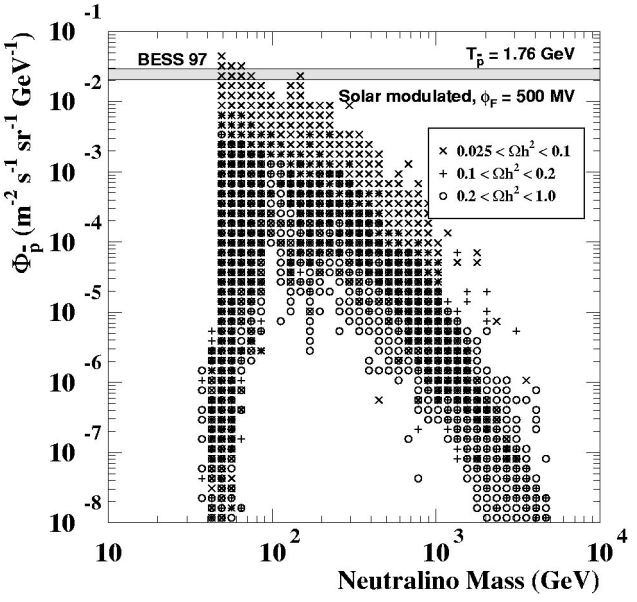

FIG. 10*b*

FIG. 10.—Solar-modulated antiproton fluxes at (*a*) 0.35 GeV and (*b*) 1.76 GeV, compared with BESS 97. The models have been coded according to their relic density, $\Omega_\chi h^2$.

Bergström, Edsjö, & Gondolo 1998a) have the added virtue of giving both a directional and a spectral signature, which can be used to improve the signal-to-background ratio well beyond the limits of present-day measurements.

The highest values for the fluxes in Figure 10*a* are 4 times higher than the BESS measurement. However, the uncertainty coming from the local halo density alone is larger than this. Given the total mass of the Galaxy, and restricting our choice of halo profile (isothermal sphere with $a = 3.5$ kpc), we find a minimal local halo density of 0.14 GeV cm^{-3}, which would correspond to a flux reduction of a factor of 4.6. To that one should add the uncertainties of the Monte Carlo simulations (up to a factor of 2) and the halo profile, the propagation model and solar modulation. For this reason it is at present not possible to exclude any supersymmetric model on the basis of antiproton measurements alone.

7.3.3. *Example of Models*

In Table 3 we show seven MSSM models that all give high $\bar{p}$ fluxes. These models have acceptable relic densities, cover a large mass range, and have varying composition (and obey present accelerator bounds).

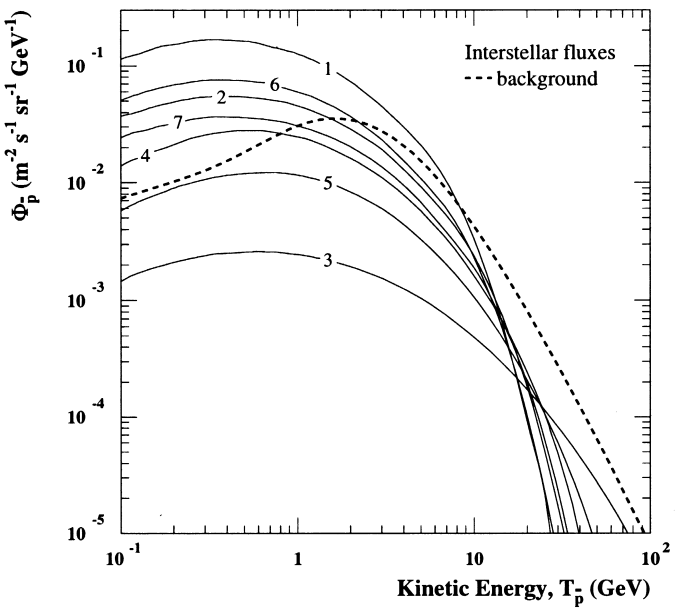

FIG. 11*a*

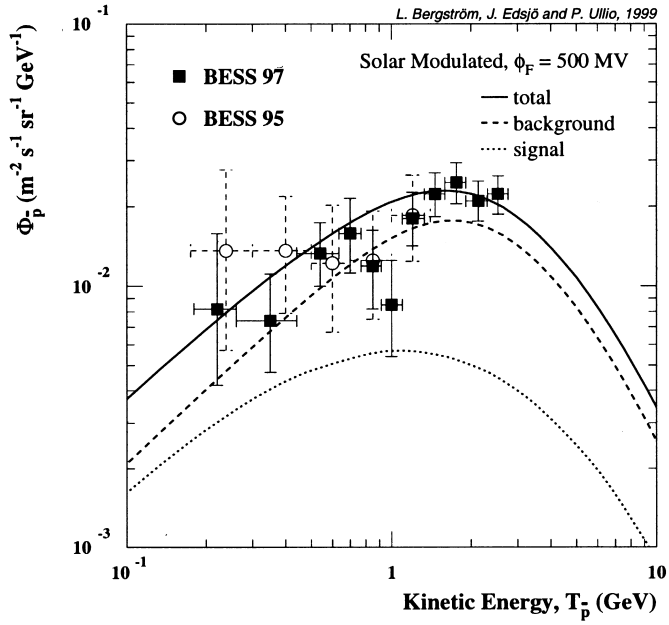

FIG. 11*b*

FIG. 11.—(*a*) Antiproton spectra for all seven models appearing in Table 3. (*b*) Example of a composite spectrum consisting of our reference background $\bar{p}$ flux (Fig. 1) reduced by 24%, with the addition of the predicted flux from annihilating dark matter neutralinos of MSSM model 5 from Table 3.

In Figure 11*a*, the predicted differential $\bar{p}$ flux is shown for the seven models. They show maxima occurring at lower energies than for our canonical background. At higher energies, the trend is that the slope of the flux decreases as the neutralino mass increases. Model 3 corresponds to a heavy neutralino, and its spectrum is significantly less steep than the background. If such a spectrum is enhanced, for instance by changing the dark matter density distribution, we would get a bump in the spectrum above 10 GeV.

In Table 3 we also show the annihilation rate and the most important branching ratios. With the help of the results in the earlier sections, the antiproton flux from neutralino annihilation can be derived. The difference between the parameterizations given in § 3.2 and the full simulation results (that we have used) is typically less than 20%.

Also note that the branching ratio to gg is never important for our high-rate models (not only the ones in the table, but all high-rate models). This is not in agreement with the results found by Jungman & Kamionkowski (1994). The reason for this difference is that we use the improved gg annihilation cross section of Bergström & Ullio (1997).

Table 3 also contains an indication of the rates for other detection methods. The neutrino-induced muon flux in neutrino telescopes does not show a strong correlation with the $\bar{p}$ flux, and it is possible to find models that give either low or high rates. Current limits are about 10^3–10^4 muons km^{-2} yr^{-1}. We also give the spin-independent neutralino-nucleon cross section (Bergström & Gondolo 1996), which should be compared with the current limits, of the order of 10^{-5} pb. These show a better, but not perfect, correlation with the $\bar{p}$ fluxes. The correlation is even stronger between the $\bar{p}$ flux and both the e^+ flux and the γ flux with continuum energy spectrum. Neither of these decrease as much with neutralino mass as the antiproton flux does, however. For more details, see Baltz & Edsjö (1999) and Bergström et al. (1999). The cross section for annihilation into monochromatic γ's (through $\gamma\gamma$ and $Z\gamma$) are uncorrelated with the $\bar{p}$ flux.

Finally, in Fig. 11*b* we show an example of a hypothetical composite spectrum consisting of our canonical background flux decreased by 24% (obtained, e.g., by decreasing the primary proton flux by 1 σ) and the signal for model 5 in Table 3. We can obtain a nice fit to the BESS data, but, as noted before, there are no special features in the spectrum that allow us to distinguish between this case and the case of no signal.

8. DISCUSSION AND CONCLUSIONS

We have seen that there is room, but no need, for a signal in the measured antiproton fluxes. We have also seen that the optimal energy to look for when searching for antiprotons is either below the solar modulation cutoff or at higher energies than currently measured. However, there are no special spectral features in the signal spectra compared to the background, unless the signal is enhanced and one looks at higher energies (above 10 GeV).

We have stressed the somewhat disappointing fact that since the present measurements by the BESS collaboration already exclude a much higher $\bar{p}$ flux at low energies than what is predicted through standard cosmic-ray production processes, an exotic signal could be drowned in this background. Even if it is not, the similar shapes of signal and background spectra will make it extremely hard to claim an exotic detection even with a precision measurement, given the large uncertainties in the predicted background flux (at least a factor of a few, up to 10 in a conservative approach). We note that some of the uncertainties might be reduced if an extrasolar probe aimed at low-energy detection were launched, a possibility that has recently been proposed (Wells et al. 1998).

Although it is tempting to conclude that what has been measured by the BESS experiment is the standard cosmic-ray–induced background flux of antiprotons, one should keep in mind that it could, on the contrary, be almost entirely due to an exotic source such as neutralino annihilation. Since this possibility cannot be excluded (at least until the problem of the dark matter in the Galactic halo has been solved), one must be cautious about using the measured antiproton flux to deduce properties of antiproton propagation and, as has recently been done (Geer & Kennedy 1998), the antiproton lifetime. We have checked that, using one of our high-mass neutralino models and a clumpy distribution of dark matter in the halo, we can get an excellent fit to the BESS data for antiproton lifetimes as low as 10^5 yr, clearly violating the claimed lower bound of Geer & Kennedy (1998). (For details, see Ullio 1999.)

We thank Mirko Boezio, Alessandro Bottino and collaborators, Per Carlson, and Tom Gaisser for useful discussions, Paolo Gondolo for collaboration on many of the numerical routines used in the supersymmetry part of the paper, and Markku Jääskeläinen for discussions at an early stage of this project. L. B. was supported by the Swedish Natural Science Research Council (NFR).

REFERENCES

Adriani, O., et al. 1995, Proc. 24th Int. Cosmic-Ray Conf. (Rome), 3, 591
Ahlen, S., et al. (The AMS Collaboration). 1994, Nucl. Instrum. Methods, A350, 351
Alam, M. S., et al. (The CLEO Collaboration). 1995, Phys. Rev. Lett., 74, 2885
Ammar, R., et al. (The CLEO Collaboration). 1993, Phys. Rev. Lett., 71, 674
Baltz, E. A., & Edsjö, J. 1999, Phys. Rev. D, 59, 023511
Berezinskii, V. S., Bulanov, S., Dogiel, V., Ginzburg, V., & Ptuskin, V. 1990, Astrophysics of Cosmic Rays (Amsterdam: North Holland)
Bergström, L., Edsjö, J., & Gondolo, P. 1998a, Phys. Rev. D, 58, 103519
Bergström, L., Edsjö, J., Gondolo, P., & Ullio, P. 1999, Phys. Rev. D, 59, 043506
Bergström, L., & Gondolo, P. 1996, Astropart. Phys., 5, 263
Bergström, L., & Ullio, P. 1997, Nucl. Phys. B, 504, 27
Bergström, L., Ullio, P., & Buckley, J. H. 1998b, Astropart. Phys., 9, 137
Boezio, M., et al. 1999, ApJ, 518, 457
Bottino, A., Donato, F., Fornengo, N., & Salati, P. 1998, Phys. Rev. D, 58, 123503
Bottino, A., Favero, C., Fornengo, N., & Mignola, G. 1995, Astropart. Phys., 3, 77
Bottino, A., Fornengo, N., Mignola, G., Olechowski, M., & Scopel, S. 1997, Astropart. Phys., 6, 395
Brückner, W., et al. 1986, Phys. Lett. B, 166, 113
Buffington, A., et al. 1981, ApJ, 248, 1179
Carena, M., Espinosa, J. R., Quirós, M., & Wagner, C. E. M. 1995, Phys. Lett. B, 355, 209
Carr, J., & The ALEPH Collaboration. 1998, preprint (ALEPH 98-029)
Caso, C., et al. (Particle Data Group). 1998, European Phys. J., C3, 1
Chardonnet, P., Mignola, G., Salati, P., & Taillet, R. 1996, Phys. Lett. B, 384, 161
Chen, X., & Kamionkowski, M. 1998, JHEP, 07(1998)001
Chiba, J., et al. 1993, Nucl. Phys. A, 553, 771c
Diehl, E., Kane, G., Kolda, C., & Wells, J. 1995, Phys. Rev. D, 52, 4223

Drees, M., Jungman, G., Kamionkowski, M., & Nojiri, M. M. 1994, Phys. Rev. D, 49, 636
Drees, M., Nojiri, M. M., Roy, D. P., & Yamada, Y. 1997, Phys. Rev. D, 56, 276
Edsjö, J. 1997, Ph.D. thesis, Uppsala Univ. (preprint hep-ph/9704384)
Edsjö, J., & Gondolo, P. 1997, Phys. Rev. D, 56, 1879
Eisenhandler, E., et al. 1976, Nucl. Phys. B, 113, 1
Ellis, J., Flores, R. A., Freese, K., Ritz, S., Seckel, D., & Silk, J. 1988, Phys. Lett. B, 214, 403
Fisk, L. A. 1971, J. Geophys. Res., 76, 221
Gaisser, T. K. 1990, Cosmic Rays and Particle Physics (Cambridge: Cambridge Univ. Press)
Gaisser, T. K., & Schaefer, R. K. 1992, ApJ, 394, 174
Garcia-Munoz, M., Simpson, J. A., Guzik, T. G., Wefel, J. P., & Margolis, S. H. 1987, ApJS, 64, 269
Geer, S. H., & Kennedy, D. C. 1998, preprint (astro-ph/9812025)
Ginzburg, V. L., Khazan, Ya. M., & Ptuskin, V. S. 1980, Ap&SS, 68, 295
Ginzburg, V. L., & Syrovatskii, S. I. 1964, The Origin of Cosmic Rays (London: Pergamon)
Gleeson, L. J., & Axford, W. I. 1967, ApJ, 149, L115
———. 1968, ApJ, 154, 1011
Glenn, S., et al. 1999, Proc. 29th Int. Conf. on High Energy Physics, ed. D. Axen & A. Astbury (Singapore: World Scientific)
Gondolo, P., & Gelmini, G. 1991, Nucl. Phys. B, 360, 145
Heinbach, U., & Simon, M. 1995, ApJ, 441, 209
Jungman, G., & Kamionkowski, M. 1994, Phys. Rev. D, 49, 2316
Jungman, G., Kamionkowski, M., & Griest, K. 1996, Phys. Rep., 267, 195
Labrador, A. W., & Mewaldt, R. A. 1997, ApJ, 480, 371
Lahanas, A. B., Tamvakis, K., & Tracas, N. D. 1994, Phys. Lett. B, 324, 387
Letaw, J. R., Silberberg, R., & Tsao, C. H. 1983, ApJS, 51, 271
———. 1993, ApJ, 414, 601
Matsunaga, H., et al. 1998, Phys. Rev. Lett., 81, 4052
Menn, O., et al. 1997, Proc. 25th Int. Cosmic-Ray Conf. (Durban), 3, 409
Mori, M. 1997, ApJ, 478, 225
Navarro, J. F., Frenk, C. S., & White, S. D. M. 1996, ApJ, 462, 563
Orito, S. 1999, Proc. 29th Int. Conf. on High Energy Physics, ed. D. Axen & A. Astbury (Singapore: World Scientific)
Ormes, J. F., & Protheroe, R. J. 1983, ApJ, 272, 756
Pierce, D., & Papadopoulos, A. 1994a, Phys. Rev. D, 50, 565
———. 1994b, Nucl. Phys. B, 430, 278
Porter, T. A., & Protheroe, R. J. 1997, J. Phys. G., 23, 1765
Protheroe, R. J. 1981, ApJ, 251, 387
Ptuskin, V. S., Völk, H. J., Zirakashvili, V. N., & Breitschwerdt, D. 1997, A&A, 321, 434
Schramm, D. N., & Turner, M. S. 1998, Rev. Mod. Phys., 70, 303
Schröter, A., et al. 1993, Nucl. Phys. A, 553, 775c
———. 1994, Z. Phys., A350, 101
Seo, E. S., & Ptuskin, V. S. 1994, ApJ, 431, 705
Sibirtsev, A., Cassling, W., Lykasov, G. I., & Rzjanin, M. V. 1997, preprint (nucl-th/9710044)
Silk, J., & Srednicki, M. 1984, Phys. Rev. Lett., 50, 624
Simon, M., & Heinbach, U. 1996, ApJ, 456, 519
Simon, M., Molnar, A., & Roesler, S. 1998, ApJ, 499, 250
Sjöstrand, T. 1994, Comput. Phys. Commun., 82, 74
Stecker, F. W., Rudaz, S., & Walsh, T. F. 1985, Phys. Rev. Lett., 55, 2622
Stecker, F. W., & Tylka, A. J. 1989, ApJ, 336, L51
Strong, A. W., & Moskalenko, I. V. 1998, ApJ, 509, 212
Tan, L. C., & Ng, L. K. 1982, Phys. Rev. D, 26, 1179
———. 1983, J. Phys. G., 9, 227
Ullio, P. 1999, preprint (astro-ph/9904086)
Ullio, P., & Bergström, L. 1998, Phys. Rev. D, 57, 1962
Webber, W. R., Lee, M. A., & Gupta, M. 1992, ApJ, 390, 96
Webber, W. R., & Potgieter, M. S. 1989, ApJ, 344, 779
Wells, J. D., Moiseev, A., & Ormes, J. F. 1998, preprint (astro-ph/9811325)
Zirakashvili, V. N., Breitschwerdt, D., Ptuskin, V. S., & Völk, H. J. 1996, A&A, 311, 113